Appl Petrochem Res (2014) 4:95–136
DOI 10.1007/s13203-014-0057-y

KACST FORUM

The catalytic stability of some selected bifunctional nanoporous-based catalysts in the hydroisomerisation of n-C7 and the effect of post-synthesis modification techniques

Faisal M. Alotaibi · Raed H. Abudawood · Hamid A. Al-Megren · Mohammed C. Al-Kinany · Essam H. Jamea · Arthur A. Garforth

Received: 5 February 2014 / Accepted: 20 March 2014 / Published online: 4 April 2014

Abstract In this work, some commercial and in-house nanoporous-based catalysts, such as USY, beta and mordenite zeolites, and mesoporous aluminosilicate molecular sieves such as MCM-48 and SBA-15, loaded with metals and acting as mono- and bimetallic bifunctional catalysts, were used for hydroisomerisation experiments in a fixed-bed reactor at pressures between 1 and 15 bar and at feed space time ranging from 2.57 to 10.26 h^{-1} (35.14–140.6 kg s mol^{-1}) to hydroisomerise *n*-heptane over a temperature range of 210–270 °C. The effect of post-synthesis treatments of micro- and mesoporous catalysts was examined, regarding their activity, selectivity and stability, such as acid and steam dealumination techniques, acid leaching via a chelating agent, bimetal loading techniques, different platinum loading methods, and composite or hybrid catalyst generation. Results show that pore architecture is the most important factor affecting coke formation and deactivation in zeolite catalysts. It was found that those catalysts with high Si/Al ratios and those which had been acid-leached or steamed showed better activity, higher selectivity towards isomeric products and better time stability. Moreover, the balance between the number of metal sites and the number of acid sites played an important role in determining the activity, selectivity and stability of the bifunctional catalysts. Higher metal loading improves catalytic stability, due to a better balance and closeness of the catalytic functions. Moreover, the bimetallic catalyst improves the formation of smaller metal particles and better dispersion, which may affect selectivity and stability.

Keywords The time-on-stream stability · Alkanes' hydroisomerisation · Catalyst deactivation · Zeolites · Bifunctional catalysts · Nanoporous catalysts · Bimetallic catalysts

F. M. Alotaibi (✉) · H. A. Al-Megren · M. C. Al-Kinany
Petrochemicals Research Institute, King Abdulaziz City for Science and Technology (KACST), P.O.Box 6086, Riyadh 11442, Saudi Arabia
e-mail: fmsalotaibi@kacst.edu.sa

R. H. Abudawood
Research and Development Center, Saudi Aramco, Dhahran 31311, Saudi Arabia

E. H. Jamea
SABIC Technology Center, Saudi Basic Industries Corporation, Riyadh 11551, Saudi Arabia

A. A. Garforth
School of Chemical Engineering and Analytical Science, The University of Manchester, Manchester M13 9PL, UK

Introduction

Tailoring catalysts to optimise their chemical, physical and mechanical features is the most widely used method of limiting a reduction in catalytic activity. With relatively slow coke formation, the fine tuning of the strength and density of acid sites in zeolites is essential to achieve a sufficiently high activity for the desired reaction. Furthermore, limitations to the diffusion of reactant, product and coke precursor molecules can be reduced by the creation of mesoporosity within zeolite crystals to produce nano-sized crystals, which will slow down coke formation. Appropriate selection of operating conditions is a crucial factor in promoting desorption of the desired products and thus limiting deactivation of the catalyst [1].

Despite the inevitable loss of catalytic activity (catalyst deactivation) in most industrial processes, there are many

ways to minimise this process and thus extend the lifetime of a catalyst. As the old saying goes, "an ounce of prevention is worth a pound of cure" [2]. The zeolite pore architecture has been found to play an important role for both the deactivation rate as a result of coking and also the composition of the carbonaceous deposits, such that zeolites with relatively large supercage pore systems, such as Y zeolites, are inherently favourable to coking reactions, which in turn leads to faster deactivation. In contrast, beta zeolite exhibits much better coking resistance, even though both zeolites have three-dimensional systems of channels [3].

The Pt/H-MOR catalyst is the most widely recognised example of a zeolitic isomerisation catalyst. It was first developed to isomerise smaller alkanes such as *n*-pentane and *n*-hexane for the Shell Hysomer process and can bring about a high isomer yield [4]. However, due to the strong tendency of middle paraffin isomerisation (C7–C9 carbon chain length) to undergo cracking, no hydroisomerisation process has yet been used industrially [5]. Strongly acidic zeolites such as H-mordenite have weaknesses as isomerisation catalysts due to the rapidity of their deactivation, particularly by olefinic carbonaceous species. There is therefore a great incentive for academic and industrial researchers to discover and develop new catalysts that are active, selective and able to resist deactivation [6, 7]. There have been detailed descriptions in the literature of how post-synthesis treatments by steam and acid of several zeolites can reduce the concentration of lattice aluminium and improve thermal/hydrothermal stability and catalytic performance whilst retaining the zeolite crystal structure. It must also be noted that mesopores form as a result of the dealumination of H-mordenite, significantly diminishing the coke's deactivating effect [8, 9].

The vast majority of microporous zeolites have pore diameters below 15 Å, leading to very high mass transfer limitations; hence, the intracrystalline diffusion of species inside the pores of zeolites is severely limited, which affects their catalytic activity and significantly reduces their product selectivity, because the increased residence time of the products in the zeolite pores favours undesired reactions such as over-cracking. Because of this limitation, there has been much work to find creative ways to eliminate the mass transfer problem. Moreover, the formation of mesopores can favour the formation of more branched or bulkier products. Evidently, generating a network of mesopores in zeolites crystals would offer numerous advantages for a great number of reactions [10]. Mesoporous aluminosilicate molecular sieves, such as SBA-15 and MCM-48, which have high surface area, large pore diameters and narrow pore size distribution and which possess uniform hexagonal and cubic one- and three-dimensional pore systems, respectively, are thus supposedly more resistant to pore blocking, which allows faster diffusion of reactants. However, they have been shown to be inferior to microporous zeolites in their acid strength and despite their larger pore diameters, which make them more able to deal with bulky molecules, they do not show higher activity than zeolites, e.g. in heavy oil cracking and the catalytic conversion of large molecules in vacuum gas oil and distillation residues. Thus, many significant improvements in both the hydrothermal stability and acidity of mesostructured aluminosilicates have been recently reported [11–13].

In this work, the time-on-stream (TOS) behaviour and deactivation rates of some commercial USY, beta and mordenite zeolites and mesoporous aluminosilicate molecular sieves such as Al-MCM-48 and Al-SBA-15 that have been loaded with platinum metal, with a wide range of Si/Al ratios, pore sizes and acidity characteristics, are evaluated in the hydroisomerisation of n-C7 when reaction conditions such as temperature, pressure and contact time are varied. n-C7 was used as a representative model compound for naphtha. A number of post-synthetic methods have been adopted to improve the catalytic properties of zeolites, such as acidity, porosity and thermal and hydrothermal stability, as these modifications are hard to achieve directly during zeolite synthesis. The main methods are ion exchange, dealumination by acid leaching or acid chelating, and stabilising through hydrothermal treatment (steaming), mono- and bimetallic effects.

Experimental

Catalyst preparation

Some commercial USY, beta, mordenite, and mesoporous aluminosilicates samples were provided by different suppliers [14–20], as shown in Table 1. These zeolite supports were designed and modified by various post-synthesis techniques so that they could be used for multiple purposes; for instance, high alkane hydroconversions like cracking, isomerisation and alkylation. They were supplied in powder form without binder materials. The in-house mordenite zeolite sample was synthesised with different properties from those of the commercial mordenite samples, then post-synthesis modified by acid and steam dealumination techniques under different treatment conditions.

USY-A, USY-C, 320HOA and 350HOA samples were subjected to post-synthetic modification by treating with AHFS to remove any EFAL. Three series of bifunctional catalysts supported on 350HOA USY were also prepared: monometallic types containing only platinum or nickel were prepared by the ion-exchange method, while the method used for bimetallic ones containing both platinum and nickel was simultaneous competitive ion exchange.

Table 1 List of catalyst supports investigated in the TOS study

	Zeolite trade name	Zeolite type	Post-synthesis modification	Supplier
1	USY-A	USY	Mildly steamed	Crosfield
2	USY-C	USY	Severely steamed	Crosfield
3	320HOA	USY	Moderately steamed	Tosoh corporation
4	350HOA	USY	Moderately steamed and acid leached	Tosoh corporation
5	CP814E	BEA	As synthesised	Zeolyst international
6	Al-MCM-48	Mesoporous aluminosilicates	Aluminated by grafting	Claytec
7	Al-SBA-15	Mesoporous aluminosilicates	Aluminated by grafting	Claytec

Finally, two series of dealuminated mordenite catalysts were prepared by acid leaching under different conditions and by applying the steaming dealumination technique at different temperatures to the in-house synthesised mordenite in its ammonium form.

Hydrothermal synthesis of mordenite zeolite

The recipe for mordenite zeolite was obtained from a verified synthesis handbook [21]. Gel calculations to determine the required weights of each reactant were performed using the synthesis molar gel composition of 6 Na_2O:Al_2O_3:30 SiO_2:780 H_2O. Therefore, calculated weights of deionised water and sodium hydroxide (99 wt% NaOH) from Merck and sodium aluminate (50.9 wt% Al_2O_3 + 31.2 wt% Na_2O + 17.9 wt% H_2O) from Sigma-Aldrich were mixed in a plastic bottle until they were completely dissolved. The required amount of Ludox AS-40 colloidal silica (40 wt% silica + 60 wt% water) from Sigma-Aldrich was then added to the solution and all were stirred using a magnetic stirrer for 12 h, after which the mixture was poured into a Teflon-lined stainless-steel autoclave and heated in an oven at 180 °C for crystallisation. After 24 h crystallisation time, the mixture was taken out of the oven, decanted and centrifuged several times while washing with deionised water after each centrifugation until the pH of the decanted solution dropped below 9. Finally, the samples were dried at 110 °C overnight until they were ready for characterisation. The optimum mordenite phase with the highest purity and crystallinity was optimised against some synthesis parameters while keeping the composition ratio of Na_2O–Al_2O_3–SiO_2–H_2O constant at the above molar gel composition. Three factors were optimised: the ageing time of the synthesis gel, the crystallisation time and the crystallisation temperature. It was found that the optimum synthesis conditions were an ageing time of 12 h, crystallisation time of 24 h and crystallisation temperature of 180 °C. This procedure was repeated more than 10 times and reproducible results were obtained, in terms both of the yields, crystallinity, bulk and framework Si/Al ratio and of the crystal morphology and size.

Post-synthesis modification techniques

Ion exchange

The procedure of ion exchange is carried out simply by immersing zeolite in a solution of the salt of the targeted cation at room temperature or a higher temperature if the exchange rate is to be improved [22], since the Brønsted acid site is generated after the modification of the parent zeolite in its sodium form by first exchanging the sodium ion with ammonium, then calcining the zeolite in the ammonium form at high temperatures to transform it into the hydrogen form. One gram of the parent commercial zeolites in their sodium form—320HOA and CBV10A—and in-house as-synthesised mordenite zeolite were dissolved in 100 ml of 0.5 M ammonium nitrate, (99 wt% purity, Sigma-Aldrich) and heated at 80 °C under reflux conditions and constant stirring for 1 h. This process was performed three times (multiple ion exchange) assuming a complete uptake of ammonium in the catalysts. The mixtures obtained were centrifuged, washed with deionised water until pH was 7, then dried at 100 °C overnight. After three ion exchanges, residual Na was determined by inductively coupled plasma (ICP) elemental analysis to be below 0.05 wt%.

Acid leaching

The treatment of zeolites by acid leaching leads to dealumination, which generally improves their efficiency in processes that result in rapid catalyst deactivation through coking, such as cracking. Acid leaching results in an increase in the Si/Al ratio through the removal of tetrahedral aluminium atoms from the framework and the subsequent introduction of mesopores into the structure, thus enhancing the thermal stability of the zeolite. It has the advantage of not forming EFAL inside the zeolite structure, as happens when Al is removed by steaming [23–26]. Acid attack was carried out by heating a suspension of in-house as-synthesised mordenite in its ammonium form (NH_4-MOR) in nitric acid or hydrochloric acid (BDH Chemicals) under reflux conditions and constant stirring under the acid leaching conditions listed in Table 2. The suspension was then filtered, washed with distilled water and dried at 110 °C overnight until it was ready for characterisation.

Table 2 Conditions of acid leaching by mineral acids

Condition	NH_4-MOR (wt)	Acid type	Acid conc. (molar)	Acid, vol. (ml)	Leaching time (h)	Temp (°C)
1	1	HCl	6	50	12	25
2	1	HCl	6	50	24	25
3	1	HCl	6	100	24	25
4	1	HCl	12.1 (conc)	100	24	120
5	1	HNO_3	10	100	16	25
6	1	HNO_3	6	50	24	25
7	1	HNO_3	15.8 (conc)	100	24	25
8	1	HNO_3	15.8 (conc)	50	24	25
9	1	HNO_3	15.8 (conc)	100	24	120
10	1	HNO_3	6	100	24	120
11	1	HNO_3	6	100	48	120
12	2	HNO_3	10	100	24	120
13	1	HNO_3	10	100	16.5	120
14	1	HNO_3	10	100	48	120
15	1	HNO_3	10	100	87	120
16	1	HNO_3	10	100	168	120

Table 3 Conditions of acid leaching by AHFS

Sample	AHFS, wt (g)	320USY, wt (g)	Mixing time (h)	Temp (°C)	Mixture volume (ml)
Optimising the mixture volume					
F1	0.6	2	1	25	25
F2	0.6	2	1	25	50
F3	0.6	2	1	25	75
F4	0.6	2	1	25	100
Optimising the mixing time					
F2	0.6	2	1	25	50
F5	0.6	2	3.5	25	50
F6	0.6	2	7	25	50
F7	0.6	2	14	25	50
Optimising the AHFS weight					
F8	0.3	2	1	25	50
F2	0.6	2	1	25	50
F9	1.2	2	1	25	50
Optimising the mixture temperature					
F2	0.6	2	1	25	50
F10	0.6	2	1	50	50
F11	0.6	2	1	75	50
F12	0.6	2	1	100	50

AHFS solution was used to remove EFAL from the USY samples: USY-A, USA-C, 320HOA and 350HOA. The 320HOA sample containing 2 wt% sodium with the ammonium form as the starting material was fine tuned using AHFS as a chelating compound to provide the best conditions to remove only the EFAL whilst maintaining the aluminium framework and original zeolite crystallinity. Thus, four main factors were considered when optimising the chemical treatments: the AHFS and USY mixture volume, the treatment duration time, the zeolite-to-AHFS weight ratio and the temperature of chemical treatment, as shown in Table 3. The zeolite-to-AHFS mass ratio was optimised in the range of 1.67–6.67. For AHFS treatments, 2 g of the steamed zeolite USY samples was placed in AHFS (99.999 % trace metals basis, Sigma-Aldrich) solution and the suspension was heated to the required temperature and stirred whilst being heated with refluxing. The suspension was filtered, washed by warm deionised water to remove any residual fluoride species until pH was 7, and then dried at 100 °C overnight. The solid obtained was subjected to three ion exchanges in ammonium nitrate solution in order to eliminate sodium and any residual fluoride species.

Steaming

Steaming or hydrothermal treatment dealumination involves calcining zeolites in the ammonium (or hydrogen) form, in the presence of steam at high temperatures. This results in the removal of aluminium atoms from the zeolite framework and their replacement by silicon atoms, thus increasing the Si/Al ratio of the framework. However, the aluminium atoms which have been removed remain in the zeolite as EFAL species, which can lead to enhanced acidity through the formation of Lewis acid sites [23]. The formation of EFAL species occurs through the migration of aluminium from the framework into the outer surface of crystals and is rate-controlled, which means that it can be accelerated or slowed down by changing the steaming temperature [27]. The in-house as-synthesised NH_4-MOR was dealuminated by steaming at 500, 600 and 700 °C for 12 h at each steaming temperature, using a fixed-bed laboratory microreactor. Deionised water was fed to the reactor using a high-performance liquid chromatography (HPLC) pump at a controlled flow rate of 0.125 ml min^{-1}. Nitrogen carrier gas (BOC, oxygen free) was dried by passage through a bed of molecular sieves and fed into the reactor at a controlled flow rate of 187.5 ml min^{-1} using a mass flow controller. The catalyst (1 g, bed particle size of 40 and 60 mesh) was located in the reactor between two beds of glass wool in the centre of the heated stable zone of the furnace. In a typical experiment, the NH_4-MOR was heated from ambient temperature to the required reactor temperature of 500 °C at a rate of 3 °C min^{-1} in a flow of air (50 ml min^{-1}) at ambient pressure for 2 h. When these conditions had stabilised, the water was introduced to the

reactor. At the end of the required time period (12 h for steaming), the water feed was stopped and the catalyst was then cooled in a stream of dry nitrogen.

Metal loading

Metals from group VIII, such as platinum and nickel, are commonly loaded onto the zeolites used in commercial refining processes as bifunctional catalysts, having both a hydrogenation/dehydrogenation function provided by the metal and an acidic function provided by the zeolite acid sites [28, 29]. A common method for preparing bifunctional catalysts is a multi-step process consisting mainly of the deposition of a metal precursor compound over the support surface, either by impregnation, ion exchange or mechanical mixing; the drying and calcination of the catalysts; and the transformation of the precursor compound into the active metallic phase by reduction. It is well established that the metal dispersion and thus the metal/acid ratio depend markedly on the way the metal is introduced [30]. The catalysts listed in Table 1 were loaded with 1 wt% platinum via the ion-exchange technique using an amino complex of platinum, and were fully described in a previous work [29–31]. The CP814E catalyst was loaded with 1 wt% platinum by wet impregnation using tetraammine platinum (II) chloride, at room temperature with excess solution under constant stirring overnight, followed by evaporation at 70 °C and drying at 110 °C. A series of monometallic and bimetallic bifunctional catalysts was formed by loading 350HOA USY with different amounts of platinum, nickel and platinum–nickel by competitive ion exchange. The first series comprised monometallic bifunctional catalysts containing 0.5, 1, 1.5 and 2 wt% of platinum, the second was a series of monometallic bifunctional catalysts containing 0.5, 1, 1.5, 2, 10 and 20 wt% of nickel and the third series was of bimetallic bifunctional catalysts containing 1 wt% of platinum and 0.25, 0.5, 0.75 and 1 wt% of nickel. The monometallic catalysts were prepared using the ion-exchange method, while the method used for the bimetallic catalysts was simultaneous competitive ion exchange, which means that the platinum and nickel precursors, $Pt(NH_3)_4Cl_2H_2O$ and $Ni(NO_3)_26H_2O$ (Fischer Chemical, 98 % purity), respectively, were mixed with the zeolite at the liquid-to-solid ratio of 50 (1 g of zeolite to 50 ml of the metal complex solution), using ammonium hydroxide solution to adjust the pH of the suspension obtained at >9.

Composite catalysts

Two composite bifunctional catalysts consisting of beta and USA zeolites were prepared as follows: (1) the 1 wt% Pt/CP814E and 1 wt% Pt/USY-C catalysts were mixed physically at a mass ratio of 1:1; (2) CP814E and USY-C in their ammonium forms were mixed at a mass ratio of 1:1 and were loaded by 1 wt% Pt using the ion-exchange method.

Catalyst characterisation

Characterisation techniques used were ICP optical emission spectroscopy (ICP–OES), X-ray diffraction (XRD), ^{27}Al and ^{29}Si MAS-solid-state NMR, pyridine adsorption Fourier transform infrared spectroscopy, ammonia temperature programmed desorption (NH_3-TPD), scanning electron microscopy and energy dispersive X-ray analysis (SEM), transmission electron microscopy (TEM), X-ray photoelectron spectroscopy (XPS), hydrogen chemisorption of platinum, BET surface area analysis by nitrogen adsorption, and thermogravimetric analysis (TGA).

Catalyst loading and testing

It was fully described in a previous work [31].

Results and discussion

Deactivation behaviour of 320HOA USY zeolite

320HOA USY zeolite was supplied by Tosoh Corporation in the form of a white powder with particle sizes between 6 and 10 μm [15]. Figures 1 and 2 show the XRD pattern and SEM microgram of 320HOA USY, respectively, and Table 4 shows the in-house characterisation of 320HOA USY using various techniques.

USY zeolite structure was confirmed from the XRD pattern for a fresh sample with 2 wt% sodium content as supplied, 320HOA USY has a lower crystallinity but a

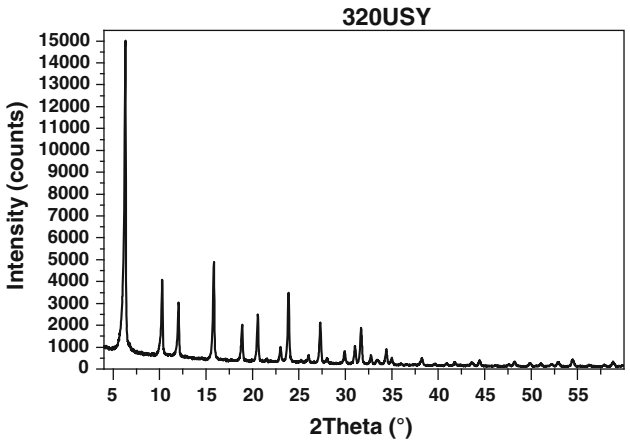

Fig. 1 XRD pattern of 320HOA USY

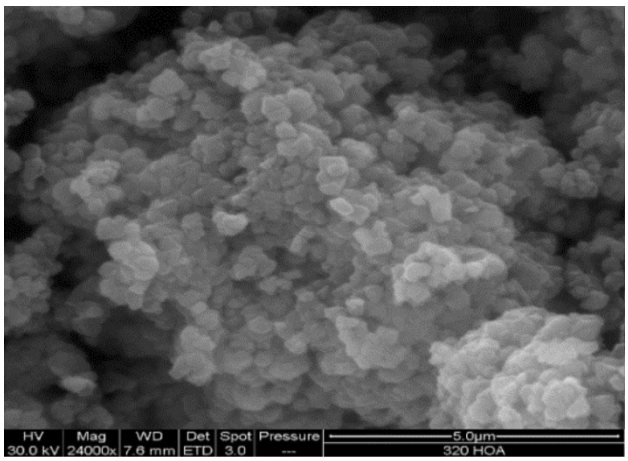

Fig. 2 SEM micrograph of 320HOA USY

higher unit cell size compared with CBV712 USY and CBV720 USY as explained in the previous work [31]. This can be related to the fact that 320HOA USY was produced via less steaming dealumination process and that no acid leaching was applied afterwards, which can be confirmed by the lower bulk Si/Al molar ratio. As a result, a reduced amount of unit cell size shrinking occurred. The rounded edged cubic crystallites, ranging in size between 1 and 3 μm, are combined with an amorphous phase which normally surrounds the zeolite Y crystals after the dealumination process, as is confirmed by the SEM images shown in Fig. 2. The ^{27}Al solid-state NMR for this USY catalyst, as shown in Fig. 3, indicated the presence of non-framework aluminium species as penta- and octa-coordinated aluminium, besides the tetrahedral aluminium framework. Four chemical environments were also obtained for Si, as shown in Fig. 4 for the ^{29}Si NMR solid state, which confirms that a shorter dealumination process was necessary to produce 320HOA USY. In addition, the Si/Al molar ratio for the framework was calculated to be 6.3, compared with 8.34 and 31.2 for CBV712 and CBV720 USY, respectively. Moreover, the ^{27}Al NMR peaks shapes and their corresponding chemical shifts were totally different from those for CBV712 and CBV720 USY, which may be explained by the different dealumination conditions that were applied to create these catalysts in the different structures. It can be concluded that most USY catalysts

Table 4 In-house characterisation of 320HOA USY

Elemental analysis (bulk)	Before ion exchange				After ion exchange with Pt precursor as tetraammine platinum (II) chloride $(Pt(NH_3)_4Cl_2).H_2O$			
	Si/Al mole ratio		2.90		Si/Al mole ratio	2.90	Pt wt%	0.83
XPS[a]	Si	Al	Si/Al	Pt	No Pt on the surface			
atomic conc %	24.42	10.89	2.24	0				
XRD	Crystallinity				Related to in-house as-synthesised Y			
	63.68							
NMR	Si/Al mole ratio of the framework				Four chemical environments of Si-NMR: Si(0Al), Si(1Al), Si(2Al) and Si(3Al)			
	6.30				Lewis acid sites existed: $Al(OSi)_4$, $(Al(H_2O)_5)^{3+}$ and $(Al(H_2O)_6)^{3+}$			
Ammonia TPD	NH_3 desorption through TPD/mmol g^{-1}				Ammonia adsorption calorimetry followed by temperature programmed desorption			
	0.30 ± 0.01							

Hydrogen chemisorption[b]	Metal dispersion	Metallic surface area (m^2 g^{-1} metal)	Metallic surface area (m^2 g^{-1} sample)	Crystallite size (nm)
	14.89	36.77	0.36	7.61

BET[b]	Surface area (m^2 g^{-1})	Pore volume (cm^3 g^{-1})		Pore size (Å)	Shows both micro- and mesoporosity	
	735.87	0.39		34.52		
TGA for coke content in spent catalyst (mass loss wt% in air) at different reaction temperatures	210 °C	Top	0.11	250 °C	Top	0.35
		Mid	0.14		Mid	0.31
		Bot	0.10		Bot	0.30
	230 °C	Top	0.24	270 °C	Top	0.10
		Mid	0.20		Mid	0.26
		Bot	0.13		Bot	0.15

[a] LPD Laboratory Services Ltd.

[b] MCA Services

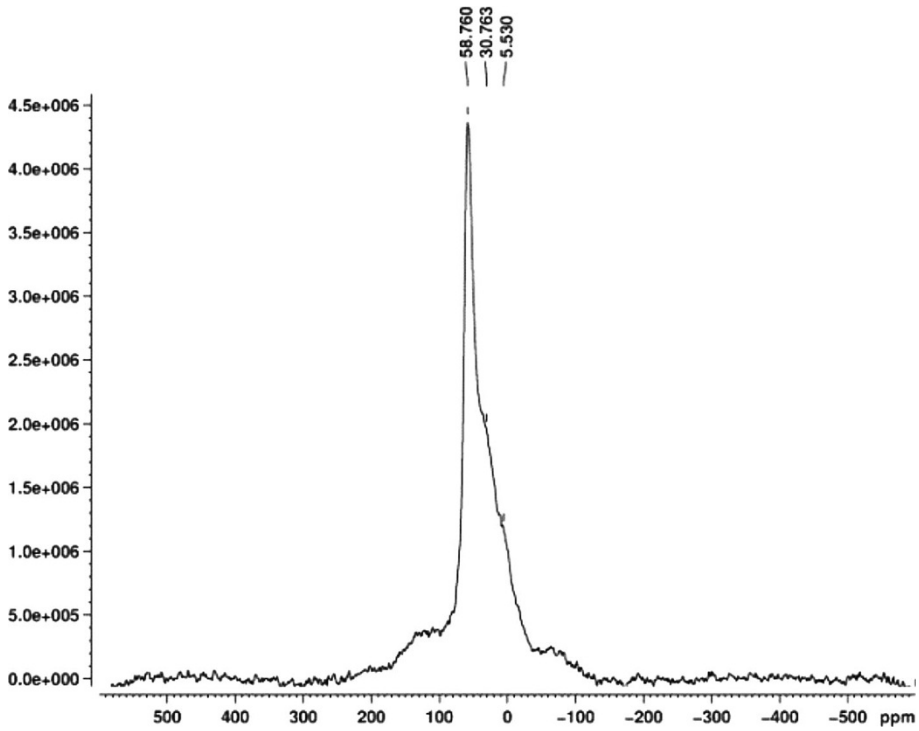

Fig. 3 ^{27}Al NMR spectra of 320HOA USY

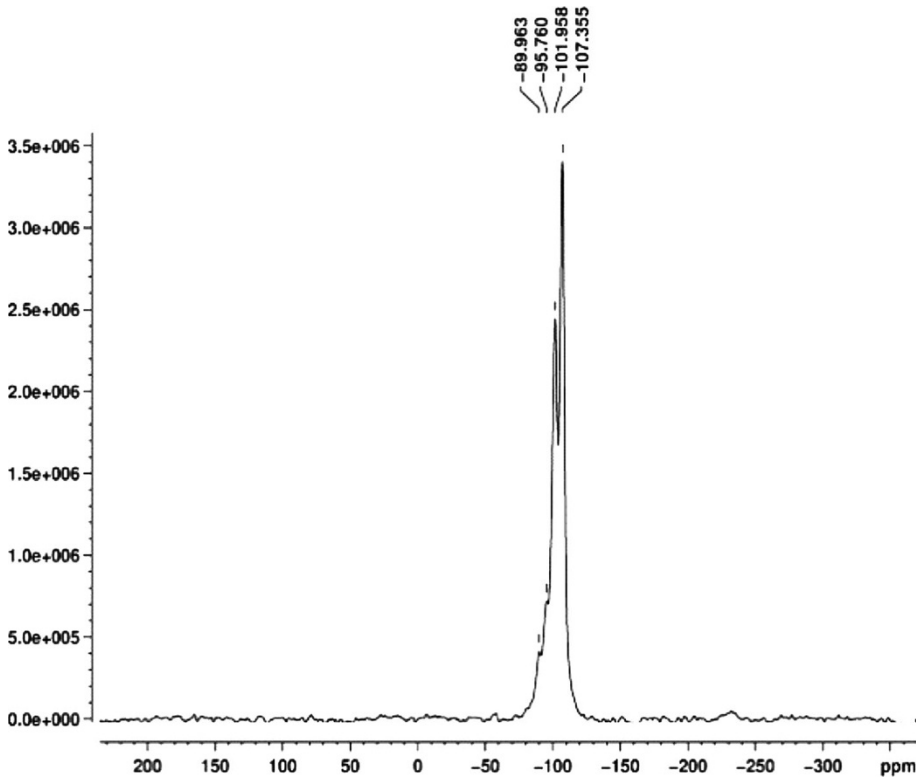

Fig. 4 ^{29}Si NMR spectra of 320HOA USY

have non-framework aluminium species; the nature and crystallographic locations within the zeolite cavities of USY catalysts are different from other catalysts, due to the dealumination conditions that have been applied to create them. Similar observations can be made for the ^{27}Al NMR peak shapes and the corresponding chemical shifts for USY-A compared with 320HOA USY as was described in [31]. They were all produced via steaming with no acid leaching, which is clearly reflected in their catalytic performance and deactivation behaviour.

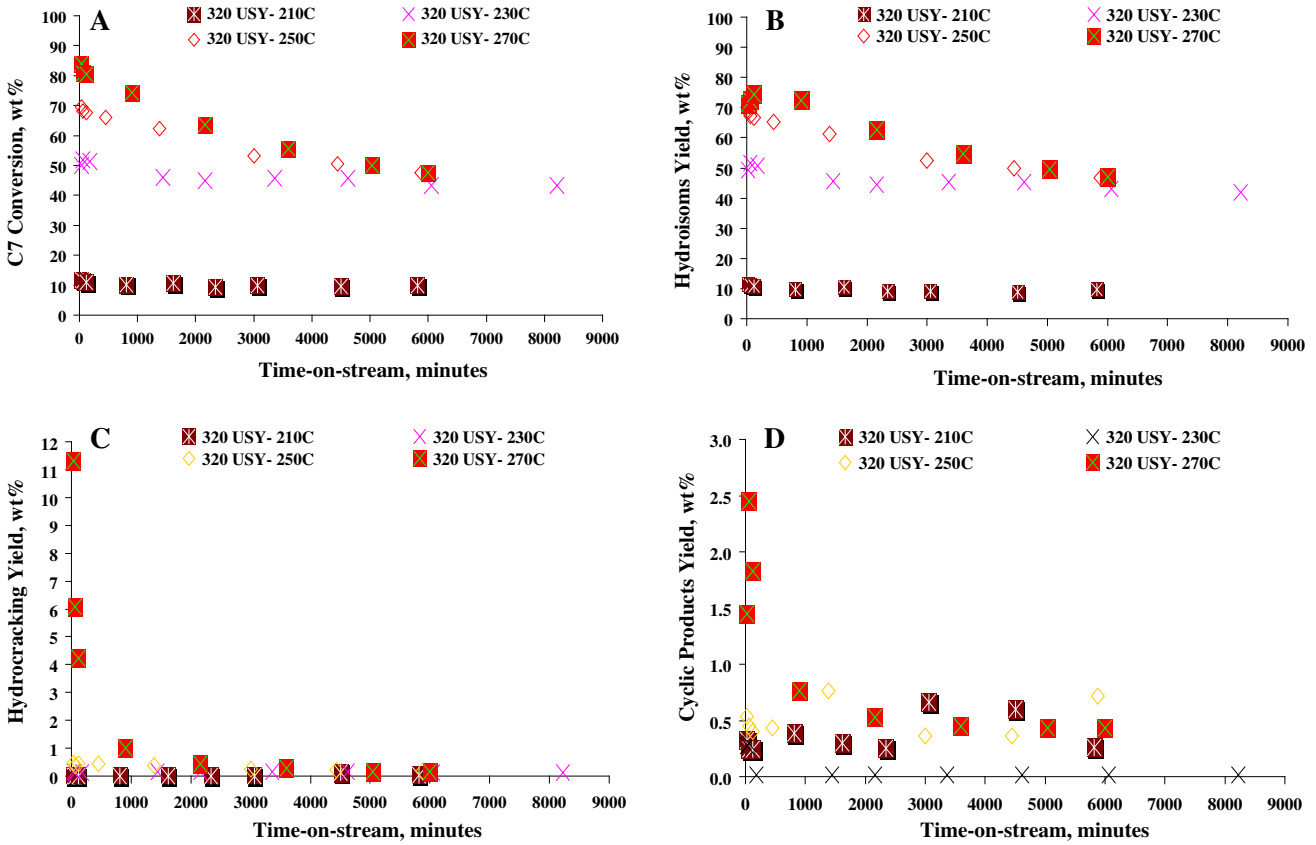

Fig. 5 Overall conversion (**a**), total yield of C7 isomers (mono + di + tribranched isomers) (**b**), total hydrocracking yield (**c**), total yield of the cyclic products (**d**) as a function of TOS for 320HOA USY at various reaction temperatures. WHSV = 5.13 h^{-1}; H_2/C7 (mol/mol) = 9; total pressure = 1 atm; temperature = 210, 230, 250 and 270 °C; 1 wt% Pt loading

The effect of TOS for the C7 conversion, hydroisomerisation, hydrocracking, and cyclic product yields at different reaction temperatures 210–270 °C are shown in Fig. 5a–d. Fresh catalyst was used for each run at each different temperature. Initially, the overall conversions were 12, 50, 70, and 84 wt% after 30 min following introduction of the feed to the reactor at the temperatures of 210, 230, 250, and 270 °C, respectively. At 210 °C, the catalyst lost about 1–2 wt% of its activity before levelling off and reaching a constant value after 60 h on stream, whereas the deactivation rate at 230 °C for the new activated catalyst was slightly faster, as can be seen in Fig. 5a. The overall conversion was 50 wt% after 30 min from the point at which the feed was introduced to the reactor, which then decreased with the TOS to 46 wt% after the first 24 h, and then decreased slowly within the deactivation rate range of 2–3 wt% every 24 h until the reaction terminated after about 6 days (140 h). A moderate drop in the catalyst activity occurred during the first few hours at the higher temperatures of 250 and 270 °C, after which a constant deactivating value was reached, ranging from 3 to 5 wt% every 24 h, until the reaction terminated. The initial selectivity towards the hydroisomerisation products was 98.5 and 84 % after 30 min following introduction of the feed to the reactor, which then increased throughout the TOS to 99 and 92 % after 120 min at 250 and 270 °C, respectively. The maximum isomer yield obtained was around 71 wt% at 270 °C and around 68 wt% at 250 °C, and selectivity towards cracked products was fairly high at the higher temperatures during the first few hours of the deactivation reaction. The highest selectivity for cracked products was 13.5 % 30 min after introducing the feed to the reactor at 270 °C, decreasing rapidly throughout the TOS and finally reaching 5 wt% after 120 min. The yield of cyclic products at the temperatures of 250 and 270 °C was also higher than at the lower temperatures.

It has been found that after the deactivation runs at temperatures of 210–270 °C, the hard coke content is lower than that found for the previously studied catalysts: CBV712USY, CBV720USY, and USY-A [31], which can be linked to the acidity properties of each catalyst. Thus, it can be seen that 320HOA USY has a lower acidity than the above catalysts resulting in a lower cracking activity and thus a lower coke formation. However, the negative effect of the presence of extra-framework Al species (EFAL) could be expected to be lower in 320HOA USY due to the pore

Table 5 The C7 conversion (wt%), product yield (wt%), and product selectivity (%) at different reaction conditions using the pressure rig for 1wt% Pt/320HOA USY

	Conversion (wt%)	Hydroisoms yield (wt%)	Hydrocrack yield (wt%)	Cyclic yield (wt%)	Hydroisoms selectivity (%)	Hydrocrack selectivity (%)	Cyclic selectivity (%)
WHSV (h^{-1})	$T = 210$ °C, $P = 1$ bar						
2.57	28.45	28.16	0.01	0.29	98.97	0.02	1.01
5.13	16.89	16.64	0.00	0.24	98.56	0.00	1.44
10.26	7.99	7.73	0.00	0.26	96.76	0.00	3.23
WHSV (h^{-1})	$T = 210$ °C, $P = 8$ bar						
2.57	3.54	3.25	0.00	0.29	91.73	0.00	8.27
5.13	4.27	3.98	0.00	0.29	93.14	0.00	6.86
10.26	0.52	0.27	0.00	0.25	52.70	0.00	47.30
WHSV (h^{-1})	$T = 210$ °C, $P = 15$ bar						
2.57	0.46	0.24	0.00	0.22	51.84	0.00	48.16
5.13	0.77	0.54	0.00	0.23	69.70	0.00	30.17
10.26	3.97	3.72	0.00	0.26	93.51	0.00	6.49
Pressure (bar)	$T = 210$ °C, WHSV = 5.13 h^{-1}						
1	16.89	16.64	0.00	0.24	98.56	0.00	1.44
8	4.27	3.98	0.00	0.29	93.14	0.00	6.86
15	0.77	0.54	0.00	0.23	69.70	0.00	30.17
WHSV (h^{-1})	$T = 230$ °C, $P = 1$ bar						
2.57	46.38	45.89	0.16	0.33	98.94	0.35	0.71
5.13	45.47	45.06	0.08	0.33	99.10	0.17	0.72
10.26	26.11	25.36	0.03	0.28	97.16	0.11	1.06
WHSV (h^{-1})	$T = 230$ °C, $P = 8$ bar						
2.57	32.35	32.00	0.04	0.31	98.91	0.13	0.97
5.13	19.90	19.56	0.03	0.31	98.29	0.16	1.55
10.26	9.08	8.80	0.00	0.28	96.94	0.00	3.05
WHSV (h^{-1})	$T = 230$ °C, $P = 15$ bar						
2.57	16.95	16.60	0.02	0.33	97.94	0.09	1.97
5.13	10.92	10.64	0.00	0.28	97.43	0.00	2.55
10.26	6.28	6.02	0.00	0.26	95.81	0.00	4.17
Pressure (bar)	$T = 230$ °C, WHSV = 5.13 h^{-1}						
1	45.47	45.06	0.08	0.33	99.10	0.17	0.72
8	19.90	19.56	0.03	0.31	98.29	0.16	1.55
15	10.92	10.64	0.00	0.28	97.43	0.00	2.55
WHSV (h^{-1})	$T = 250$ °C, $P = 1$ bar						
2.57	78.83	76.38	1.82	0.62	96.90	2.31	0.79
5.13	68.83	67.52	0.85	0.47	98.09	1.23	0.68
10.26	39.93	38.96	0.55	0.43	97.55	1.36	1.08
WHSV (h^{-1})	$T = 250$ °C, $P = 8$ bar						
2.57	70.07	68.91	0.83	0.32	98.35	1.19	0.46
5.13	52.62	51.99	0.66	0.31	98.81	1.25	0.58
10.26	30.51	30.05	0.19	0.27	98.50	0.61	0.89
WHSV (h^{-1})	$T = 250$ °C, $P = 15$ bar						
2.57	52.05	51.45	0.30	0.31	98.83	0.58	0.59
5.13	42.85	42.32	0.25	0.29	98.76	0.58	0.68
10.26	25.38	24.94	0.15	0.29	98.28	0.58	1.14

Table 5 continued

	Conversion (wt%)	Hydroisoms yield (wt%)	Hydrocrack yield (wt%)	Cyclic yield (wt%)	Hydroisoms selectivity (%)	Hydrocrack selectivity (%)	Cyclic selectivity (%)
Pressure (bar)	$T = 250$ °C, WHSV = 5.13 h^{-1}						
1	68.83	67.52	0.85	0.47	98.09	1.23	0.68
8	52.62	51.99	0.66	0.31	98.81	1.25	0.58
15	42.85	42.32	0.25	0.29	98.76	0.58	0.68
WHSV (h^{-1})	$T = 270$ °C, $P = 1$ bar						
2.57	78.02	71.93	4.18	1.91	92.19	5.36	2.45
5.13	72.53	69.68	1.88	0.97	96.07	2.59	1.34
10.26	41.78	40.09	0.96	0.73	95.94	2.31	1.75
WHSV (h^{-1})	$T = 270$ °C, $P = 8$ bar						
2.57	66.87	63.21	3.27	0.39	94.53	4.89	0.58
5.13	54.19	50.28	3.65	0.26	92.79	6.74	0.48
10.26	30.19	28.25	1.67	0.27	93.57	5.54	0.88
WHSV (h^{-1})	$T = 270$ °C, $P = 15$ bar						
2.57	58.01	54.98	2.71	0.32	94.78	4.68	0.54
5.13	43.24	40.59	2.37	0.29	93.86	5.47	0.66
10.26	29.63	27.47	1.90	0.26	92.69	6.42	0.89
Pressure (bar)	$T = 270$ °C, WHSV = 5.13 h^{-1}						
1	72.53	69.68	1.88	0.97	96.07	2.59	1.34
8	54.19	50.28	3.65	0.26	92.79	6.74	0.48
15	43.24	40.59	2.37	0.29	93.86	5.47	0.66

blockage effect, especially in the polymeric species [24], such that the coke content can be trapped within the pores since these will be smaller than those found for USY-A.

Effects of reaction pressure and contact time for 1 wt% Pt/320HOA USY

The effect of increasing the hydrogen partial pressure, and hence the overall reaction pressure and variation in contact time, representing the time taken by reactants to pass through the catalyst bed during a reaction, has been studied in this work at a range of temperatures from 210 to 270 °C for the hydroisomerisation of n-C7 over 1 wt% platinum-loaded 320HOA USY. A stainless-steel higher pressure unit was used, and the catalyst (1 wt% Pt/320HOA USY) was tested at temperatures ranging from 210 to 270 °C, WHSV of 2.57, 5.13, and 10.26 h^{-1}, and pressures of 1, 8 and 15 bar. At each temperature, products of the reaction were collected at the point where steady-state conditions were achieved; catalysts were calcined and then re-reduced before proceeding to the next temperature. Unfortunately, the reaction rig could not operate overnight at high pressures due to the necessary safety precautions and therefore it was not possible to fully study deactivation behaviours at these pressures.

Table 5 shows the results from the n-C7 conversion (wt%), product yield (wt%), and product selectivity (%) at the different reaction conditions using the pressure rig for the hydroisomerisation of n-C7 over 1 wt% Pt/320HOA USY. In general, it has been found that an increase in pressure results in a decrease in overall conversion and a slight decrease in selectivity to isomers with a noticeable increased selectivity to the cyclic products, particularly at the lower temperatures of 210 and 230 °C. There was no obvious cracking activity at the lower temperatures of 210 and 230 °C, and a constant WHSV was observed whilst changing reaction pressures. In contrast, at the highest temperature of 270 °C and WHSV of 5.13 h^{-1}, increased selectivity towards the cracked products was observed with increased reaction pressures, with comparable results being reported by Chao et al. [32] who investigated the effect of reaction pressure over the range 1–41.3 bar on mordenite catalysts with different Si/Al ratios and the zeolite Beta. In addition, they showed that pressure reduced the cracking yield for all catalysts as well as improved the mordenite catalysts' stability. Additionally, an increase in hydrogen pressure has been found to reduce the hydroisomerisation reaction rate [33], where an increase in the hydrogenation activity at higher hydrogen pressure results in the hydrogenation of intermediate olefins, due to a shorter intermediate olefin residence time inside the catalyst [34]. This minimises the cracking activity, since pressure reduces overall conversion but improves hydroisomerisation selectivity compared with that of cracking, which to some extent, was not the case for catalyst 1 wt% Pt/320HOA

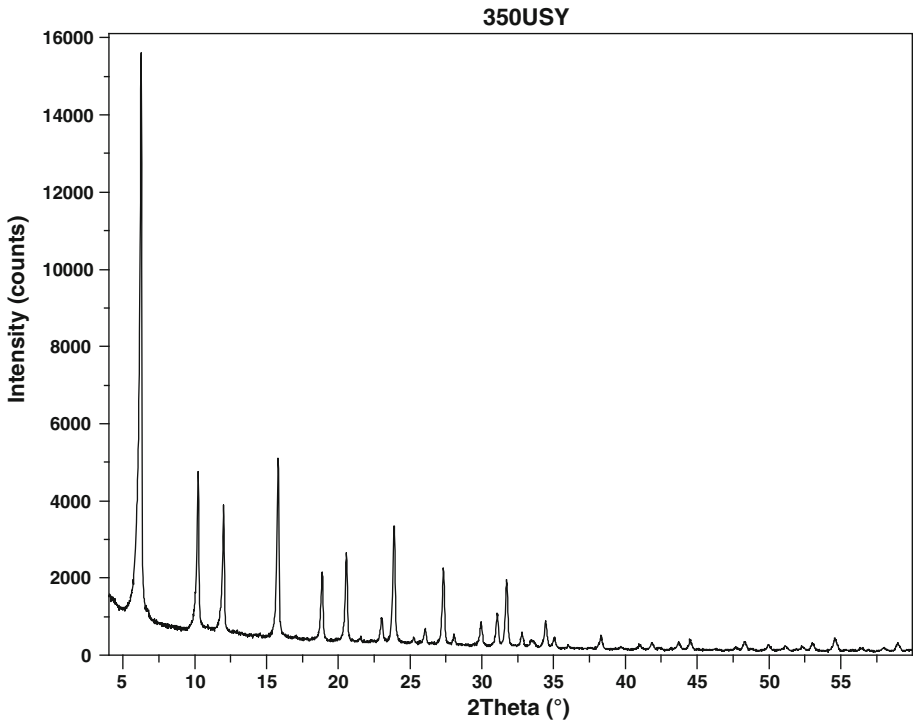

Fig. 6 XRD pattern for 350HOA USY

USY, whose small average pore diameter most likely limited the movement of larger molecules at high pressures, and therefore promoted cracking.

Table 5 illustrates that the conversion increased as the contact time increased (WHSV $\leq$ 10.26, 5.13, 2.57 h^{-1}) at constant temperature and pressure. However, increasing contact time between the reaction feed (n-C7) and the catalyst appears to cause a reduction in cyclic product yield, giving rise to an increase in cracking and hydroisomerisation selectivity.

Wang et al. [35] found that increasing the contact time results in an increased overall conversion of n-C7 at a constant temperature of 220 °C and in a reduced selectivity in hydroisomerisation versus cracking. Similar observations were made by Chica and Corma [36] when they tested the hydroisomerisation of nC_5, nC_6 and nC_7 over platinum-loaded zeolite supports. However, the decrease in selectivity to isomers was opposed by an increase in the overall yield of isomers at short contact times. It was also shown that with increasing contact times, the formation of multi-branched isomers also increases, leading to a lower mono/multi-branched isomer ratio. This behaviour could result from an initial formation of mono-branched isomers and their subsequent transformation into multi-branched isomers.

Deactivation behaviour of 350HOA USY zeolite

350HOA USY zeolite was supplied by Tosoh Corporation in the form of a white powder with particle sizes between 6 and 10 μm. The Figs. 6 and 7, respectively, show the XRD

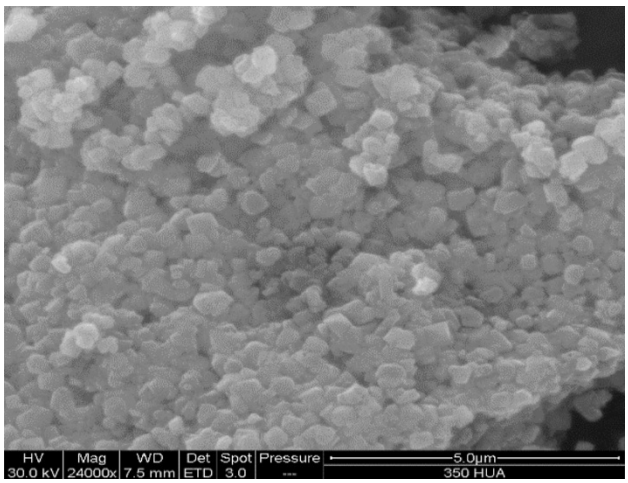

Fig. 7 SEM micrograph for 350HOA USY

pattern and SEM micrograph for 350HOA USY, and Table 6 the in-house characterisation for 350HOA USY using different techniques.

Figures 8 and 9 show solid-state NMR spectra for ^{27}Al and ^{29}Si, respectively. ^{27}Al MAS NMR analysis revealed that the catalyst had EFAL species even though it was a dealuminated and partially acid-leached zeolite. Information regarding the Si atoms coordinated (via oxygen) with neighbouring T atoms (Si and Al) is provided by ^{29}Si MAS NMR, indicating two different chemical configurations of SiO_4, which were assigned to (4Si,0Al) and SiO_4 (3Si,1Al).

This confirms that 350HOA was produced by a dealumination process and acid leached to achieve a high Si/Al

Table 6 Some in-house characterisations of 350HOA USY

Elemental analysis (bulk)	Before ion exchange				After ion exchange with Pt precursor as tetraammine platinum (II) chloride $(Pt(NH_3)_4Cl_2).H_2O$			
	Si/Al mole ratio		5.55		Si/Al mole ratio	5.55	Pt wt%	0.90
XPS[a]	Si	Al	Si/Al	Pt	Pt is likely to be metallic			
Atomic Conc %	28.32	5.69	4.98	0.07				
XRD	Crystallinity %				Related to in-house as-synthesised Y			
	66							
NMR	Si/Al mole ratio for the framework				Two chemical environments for Si-NMR: Si(0Al) and Si(1Al)			
	12.38				Lewis acid sites are present			
Ammonia TPD	NH_3 desorption through TPD/ mmol g^{-1}				Ammonia adsorption calorimetry followed by temperature programmed desorption			
	0.76 ± 0.01							

BET[b]	Surface area (m^2 g^{-1})	Pore volume (cm^3 g^{-1})		Pore size (Å)	Shows both micro and mesoporosity	
	872.97	0.47		26.10		
TGA for coke content in spent catalyst (mass loss wt% in air) after different reaction temperatures	210 °C	Top	0.10	250 °C	Top	0.26
		Mid	0.13		Mid	0.37
		Bot	0.13		Bot	0.28
	230 °C	Top	0.52	270 °C	Top	1.20
		Mid	0.76		Mid	1.12
		Bot	0.71		Bot	1.29

LPD Laboratory Services Ltd.

[b] MCA Services

mole ratio; thus a high surface area was obtained, as there were fewer EFAL species. This would result in a mesoporous channel network, due to the larger pore volume. Moreover, it should be noted that the dealumination process required to produce 350HOA USY was less severe than for the CBV720USY catalyst [31], which has a higher Si/Al mole ratio in the framework than 350HOA USY. Nevertheless, both catalysts have mesoporous systems, due to larger pore volumes and surface areas, but less acidity and thus lower catalytic activity compared to just-dealuminated catalysts.

The effects of TOS on the C7 conversion, hydroisomerisation, hydrocracking, and cyclic product yields at different reaction temperatures 210–270 °C are shown in Fig. 10a–d, respectively. Fresh catalyst was used for each run at the different reaction temperatures. Initially, the overall conversion was 17, 56, 75, and 84 wt% after 30 min from the point when the feed was introduced to the reactor at the temperatures of 210, 230, 250, and 270 °C, respectively. At 210 °C, the catalyst lost about 1–2 wt% of its activity and then reached a pseudo-stable state for the initial 60 min on stream. The deactivation rate at 230 °C for the new activated catalyst was slightly faster, with the overall conversion being 56 wt% after 30 min after which it decreased with the TOS to 51 wt% after 27 h, and then decreased slowly within the deactivation rate range of 2–3 wt% every 24 h until the reaction finally terminated after about 6 days (140 h). Rapid initial deactivation occurred during the first few hours at the higher temperatures of 250 and 270 °C, followed by a constant deactivating value being reached, ranging from 3 to 5 wt%, every 24 h until the reaction terminated.

The initial selectivity towards the hydroisomerisation products was 98 and 85 % after the initial 30 min, and then increased throughout the TOS to 99 and 94 % after 120 min at 250 and 270 °C, respectively. Thus, the selectivity towards cracked products was fairly high at higher temperatures during the first few hours of the deactivation reaction, with the highest cracked product selectivity being 14 % 30 min after introducing the feed to the reactor at 270 °C; however, this decreased rapidly throughout the TOS to 4 % after 120 min. Additionally, the yield of cyclic products at the temperatures of 210 and 230 °C was higher than that at the higher temperatures.

The TOS results provide evidence that the higher activity of 350HOA USY compared to CBV720 USY [31] is related to the number of acid sites. Furthermore, moderately slow deactivation for both catalysts was observed, reaching the pseudo-stable state in the initial few minutes at the lower temperatures of 210 and 230 °C. The n_{Pt}/n_A ratio for 350HOA USY was calculated as 0.06, which is in the suggested range of $0.03 \leq n_{Pt}/n_A \leq 0.17$ for a well-

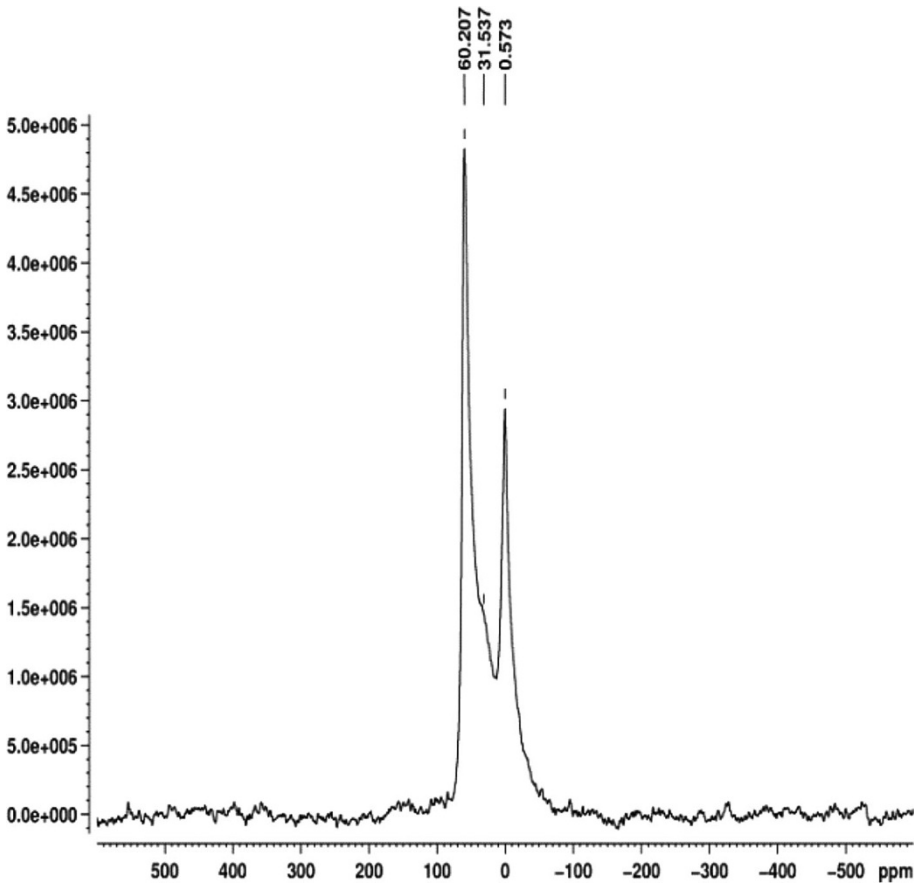

Fig. 8 ^{27}Al NMR spectra for 350HOA USY

balanced bifunctional catalyst, in conjunction with 0.12 for CBV720 USY, which allowed deactivation to occur at reasonably low temperatures with lower coke content. Although the mesoporosity texture was similar for both catalysts, the average coke content was higher for 350HOA USY, which may be due to its higher acidity, as the framework Si/Al was lower, resulting in cracking activity at temperatures of 250 and 270 °C.

Extraction of EFAL in USY zeolites by AHFS post-synthetic modification

Ammonium hexafluorosilicate solution was used to remove the EFAL from the USY samples: USY-A, USA-C, 320HOA, and from the acid-leached 350HOA, due to the samples having different silicon-to-aluminium ratios, and thus different numbers of aluminium atoms as non-framework on their crystal unit cells. As with dealumination, after the process the aluminium removed from the framework remains on the crystal and migrates to the surface in an extension that is dependent on the partial pressure of the steam used. This can be confirmed by Si/Al ratio results on the above USYs surfaces by XPS analysis as shown in Tables 4 and 6 and it can be seen that the Si/Al ratios on the surfaces are much lower for zeolites that have only been dealuminated, such as USY-A, USY-C, and 320HOA than for the acid-leached zeolites such as CBV712, CBV720 and 350HOA. The resulting AHFS modified zeolite samples were characterised by XRD, MAS NMR, ammonia TPD, ICP, XPS and BET, with the effects of the treatments on the total amount and type of EFAL, the relationship between amount and nature of acid sites, and the deactivation behaviour discussed below.

Optimisation of chelating extraction parameters

The USY sample 320HOA containing 2wt% sodium with the ammonium form as the starting material has been fine tuned using a chelate compound (ammonium hexafluorosilicate $(NH_4)_2SiF_6$) to provide the best condition to remove only the non-framework aluminium whilst maintaining the aluminium framework and original zeolite crystallinity—as these are unaffected by this chelating agent. Four main factors were considered when optimising the chemical treatments: (1) the AHFS and USY mixture volume, (2) the treatment duration time, (3) the zeolite to AHFS weight ratio, and (4) the temperature used during the chemical treatment. Table 7 lists the resulting modified sample characteristics for each factor and illustrates, for the AHFS modified samples, that the increase in mixture volume

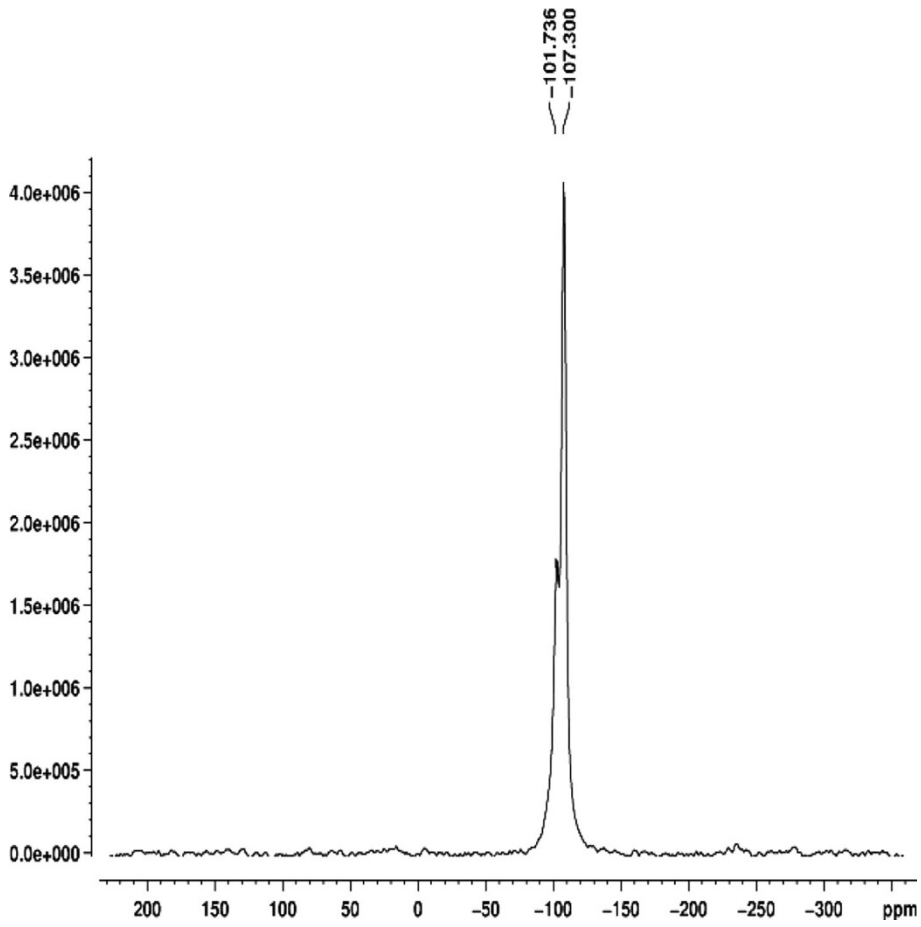

Fig. 9 ^{29}Si NMR spectra for 350HOA USY

caused the total aluminium content in the bulk to decrease from 9.73 wt% before the modification to between 4.83 and 5.51 wt%. Additionally, both the Si/Al mole ratio in the framework and the crystallinity were maintained in the ranges of 6.45–6.75 mol ratio and 57–68 %, respectively. There was no significant effect on the mixing time factors, such that the Si/Al mole ratio in the framework and the crystallinity were maintained in the ranges of 6.45–6.75 and 57–66 %, respectively. The zeolite to AHFS mass ratio was optimised in the range of 6.67–1.67, so the framework structure had been attacked by the AHFS at a ratio of 1.67 mol, leading to a Si/Al mole ratio in the framework which increased to 11.10.

A temperature range of 25–100 °C was used during the chemical treatment and it was found that the resulting modified samples had the total aluminium content in the range of 4.79–5.56 wt%, and crystallinity in the range of 57–64 %. As well as this, the framework was unaffected as the temperature rose, leaving the Si/Al in the framework in the range of 6.43–6.53 mol ratio. It can be seen that the total Si content in the modified samples is higher than that detected for the original sample 320HOA before the acid chelating treatment, which can explained by the existence of the silicon fluoride containing species on the outer surfaces of the modified zeolites, an effect that has been reported in the literature [27, 37]. The detected residual fluoride species was removed from the structure by applying an extra ammonium ion-exchange step.

Table 8 shows the unit cell for the AHFS modified samples, the starting material sample (320HOA), the total aluminium number Al_{total} (based on the elemental analysis), the framework aluminium number Al_F (measured using ^{29}Si MAS NMR $(Si/Al)_F$, and on the basis of 192 T atoms (Si or Al) per unit cell with the composition of $H_x(AlO_2)_x(SiO_2)_{192-x}$) and the EFAL number Al_{nF}, (the difference between the Al_{total} and Al_F) [26, 27, 38, 39]. To some extent, the value for $Al_{F/u.c}$ was greater than the value for the total $Al_{total/u.c}$ as shown for the samples designated as F9, F10, and F22 in the table, so this difference reflects the errors in analyses for some AHFS modified samples which may have resulted from the existence of silicon fluoride containing species during the chemical treatment. The Al_{nF} extraction efficiency percentage was calculated for each resulting sample by dividing the difference between Al_{nF} for the modified sample and Al_{nF} for the starting material, which is equal to 23 atoms for 320HOA.

It is clear from Table 8 that the most effective extraction of EFAL by AHFS chelating agent was for the samples F4,

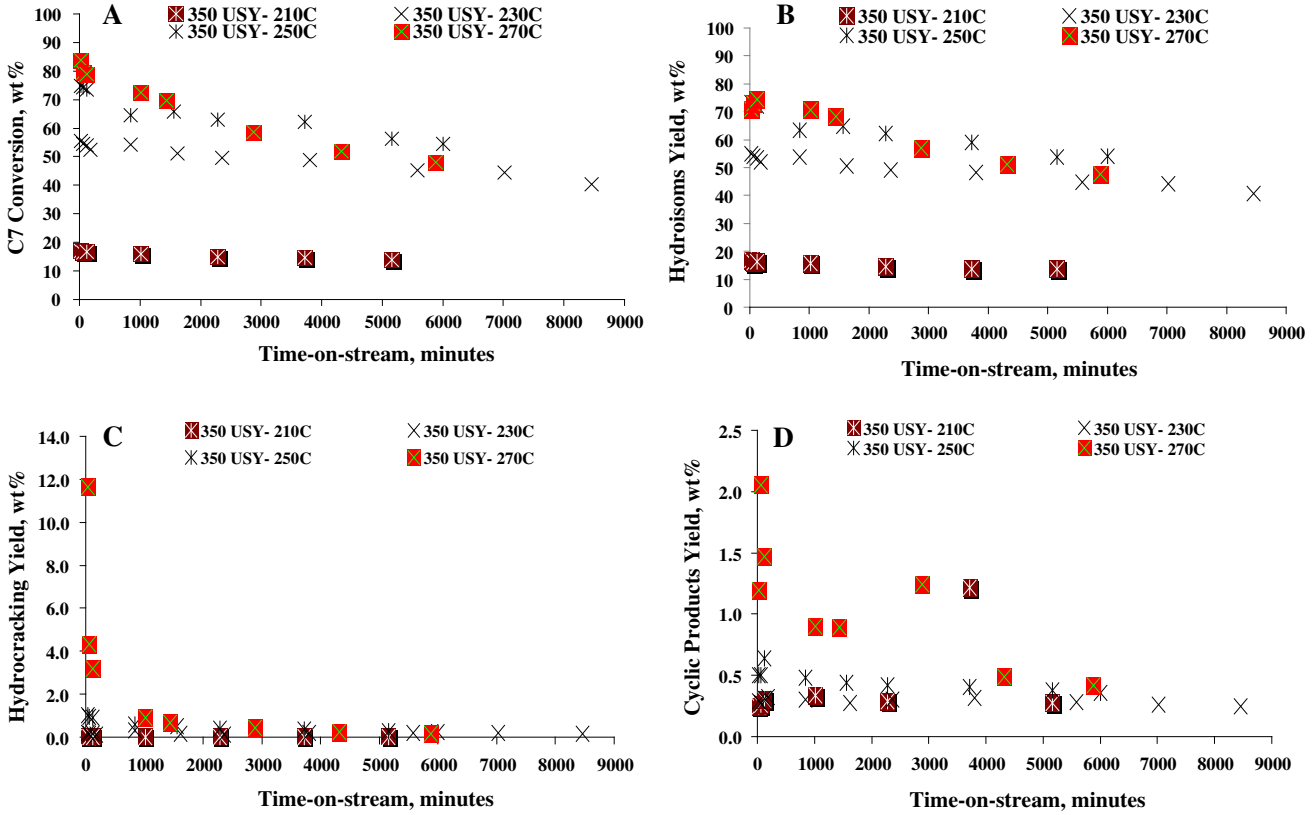

Fig. 10 Overall conversion (**a**), total yield of C7 isomers (mono + di + tribranched isomers) (**b**), total hydrocracking yield (**c**), and total yield of the cyclic products (**d**) as a function of TOS for 350HOA USY at various reaction temperatures. WHSV = 5.13 h^{-1}; H_2/C7 (molar) = 9; total pressure = 1 atm; temperature = 210, 230, 250 and 270 °C; 1 wt% Pt loading

F5, F6, F7, and F11. The results for the starting material (320HOA) are arranged in the table according to the chemical treatment conditions applied, where the EFAL formed represents approximately 47 % of the total aluminium. Furthermore, the obtained $(Si/Al)_T$ as bulk (measured by the chemical analysis) is almost in agreement with $(Si/Al)_F$ measured by NMR analysis for those samples (F4, F5, F6, F7, and F11) which has 100 % extraction efficiency. The lowest extraction efficiency was found to be 46 % for the modified sample F8, which was prepared by the chemical treatment using the highest mass ratio (6.67 wt/wt) of zeolite to AHFS, which can be considered as the mildest condition, with moderate extraction efficiency observed for the modified samples F1, F2, F3, and F12 in which partial extraction occurred, leaving the framework aluminium unaffected, and maintaining the framework $(Si/Al)_F$ ratio as prior to modification. This resulted in reasonable crystallinity values in the range of 61–66 % compared with the original crystallinity of 64 % for the starting material.

Catalysts USY-A, USY-C, 320HOA USY, and 320HOA USY were chemically treated by AHFS to remove the EFAL as these have a detrimental effect on catalytic and transport properties, and consequently adversely affects the coke formation and deactivation behaviour. The EFAL was removed from the catalysts in their ammonium form using the chelating agent AHFS under the same chemical treatment conditions as sample F2. This involved 50 ml of a solution mixture, stirred for 1 h at room temperature, with a zeolite to AHFS mass ratio of 3.33 wt/wt. From Table 9, it can be seen that samples F20 and F21, the modified samples of catalysts USY-A and USY-C, respectively, still have EFAL which has not been extracted by AHFS, and that framework Al atoms were attacked. In contrast, F2 was partially extracted but was not attacked by the AHFS. It can be interpreted that F2 was produced by the AHFS treatment of 320HOA USY which in its ammonium form contains approximately 2 wt% sodium, and thus the presence of sodium inhibits aluminium extraction [27]. Table 9 shows the in-house characterisation for the original and modified catalysts using different techniques, and it can be seen that the $(Si/Al)_F$ increased for modified samples F20 and F21, confirming that the AHFS has dealuminated the framework Al atoms, and subsequently decreased their crystallinity. It was also observed that the zeolites prepared with AHFS retained less than 0.6 wt% fluorine based on the ion chromatography analysis, which was not seen by XPS analysis measurements for the

Table 7 The chemical treatment parameters of AHFS and the resulting samples characteristics

	The chemical treatment conditions					Elemental analysis ICP			MAS NMR	XRD
	AHFSwt (g)	320USYwt (g)	Mixing time (h)	Temp (°C)	Vol (ml)	Si (wt%)	Al (wt%)	Bulk (Si/Al) (mol/mol)	Framework (Si/Al) (mol/mol)	Crystallinity (%)
320 USY	–	–	–	–	–	29.36	9.73	2.9	6.41	63.68
Optimising the mixture volume										
F1	0.6	2	1	25	25	30.01	5.51	5.23	6.71	63.57
F2	0.6	2	1	25	50	30.71	5.22	5.65	6.45	57.27
F3	0.6	2	1	25	75	31.18	5.33	5.62	6.75	66.47
F4	0.6	2	1	25	100	32.37	4.83	6.44	6.23	68.46
Optimising the mixing time										
F2	0.6	2	1	25	50	30.71	5.22	5.65	6.45	57.27
F5	0.6	2	3.5	25	50	33.12	4.75	6.70	6.75	66.28
F6	0.6	2	7	25	50	33.73	4.81	6.74	6.60	62.91
F7	0.6	2	14	25	50	33.72	4.6	7.04	6.59	66.69
Optimising the AHFS weight										
F8	0.3	2	1	25	50	30.94	7.37	4.03	6.51	60.57
F2	0.6	2	1	25	50	30.71	5.22	5.65	6.45	57.27
F9	1.2	2	1	25	50	37.68	1.68	21.55	11.10	67.11
Optimising the mixture temperature										
F2	0.6	2	1	25	50	30.71	5.22	5.65	6.45	57.27
F10	0.6	2	1	50	50	33.37	4.58	7.00	6.51	63.53
F11	0.6	2	1	75	50	32.5	4.79	6.52	6.43	64.47
F12	0.6	2	1	100	50	32.16	5.56	5.56	6.53	61.13

samples surface. In addition, the XPS measurements revealed that the surface atomic concentration for the aluminium atoms decreased for the AHFS modified samples; thus, it can observed that the $(Si/Al)_F$ mole ratio measured by NMR, (Si/Al) measured by the elemental analysis, and Si/Al measured by XPS present a closer match to each other, particularly in the case of sample F2 as opposed to samples F21 and F22 in which the Al_F was attacked by the AHFS. In terms of the obtained texture of the samples treated with AHFS, some mesoporosity developed within the crystal as the pore volume increased and pore size decreased, thus the total surface area was consequently increased for all of the modified samples.

Figure 11a–d shows the effect of TOS on the n-C7 conversion, hydroisomerisation, hydrocracking and cyclic product yields at the reaction temperature of 230 °C for the samples F2, F20 and F21, which are the AHFS modified samples for the catalysts 320HOA USY, USY-A, and USY-C, respectively. Figure 11a shows that the initial overall conversion was 63 wt% after 30 min from introducing the feed to the reactor at the temperature of 230 °C for F21 compared to 50 wt% for 320HOA USY before the modification, and that the catalyst lost about 1–2 wt% of its activity before reaching a constant "level-off" value after 60 h on stream. The deactivation rate for the F2 catalyst was slightly faster than the parent catalyst along the TOS to be in the range of 3–4 wt% and then reached a constant "level-off" value until the reaction terminated after about 4 days (5,580 min).

Figure 11b shows that the initial selectivity towards the hydroisomerisation products was 98 % for F2 compared to 99 % for 320HOA USY before the modification and kept almost the same along the deactivation run. As demonstrated in Fig. 11c and d, the selectivity towards cracked and cyclic products was fairly high for F2 in comparison with 320HOA USY which may be due to the n_{Pt}/n_A ratio being disturbed as a consequence of increasing the number of acid sites for F2.

Figure 12a shows that the initial overall conversion was 60 wt% after 30 min from the point when the feed was introduced to the reactor at the temperature of 230 °C for F20 compared to 70 wt% for USY-A before the modification [31], which is then decreasing with the TOS to 43 wt% after 780 min and decreasing slowly within the deactivation rate ranging between 1 and 3 wt% every 24 h until the reaction terminated after almost 4 days. In comparison with USY-A, which was completely deactivated in the initial few minutes, F20 deactivated much more steadily with TOS, which may be explained by the effect of pore blockage by the polymeric EFAL species being overcome even in the presence of some EFAL due to further dealumination occurring during the acid leaching

Table 8 Al content of AHFS modified samples and extraction efficiency

	Al_{total}/u.c	Al_F/u.c	Al_{nF}/u.c	Al_{nF} %	Extraction efficiency (%)
320USY	49	26	23	47	–
F1	31	25	6	19	75
F2	29	26	3	11	87
F3	29	25	4	15	82
F4	26	26	0	0	100
F5	25	25	0	0	100
F6	25	25	0	0	100
F7	24	24	0	0	100
F8	38	26	13	33	46
F9	9	16	*	*	–
F10	24	26	*	*	–
F11	26	26	0	0	100
F12	29	26	4	13	84
USY-A	50	24	26	52	**
F20	24	18	6	25	**
USY-C	51	22	29	57	**
F21	24	15	9	38	**
350USY	29	14	15	52	**
F22	5	13	*	*	–

* This difference reflects the errors in the analyses. ** Al_F attacked by AHFS

via the AHFS chelating agent. Figure 12b illustrates that the initial selectivity towards the hydroisomerisation products was 97 % for F20 compared to 92 % for USY-A before the modification and was maintained fairly steadily along the deactivation run. As shown in Fig. 12c, d, the selectivity towards cracked and cyclic products was fairly high for F20 compared with USY-A, which may be due to the n_{Pt}/n_A ratio being disturbed as a consequence of increasing the number of the acid sites (n_A) for F20, and also due to the presence of some EFAL species.

From the Fig. 13a, the initial overall conversion was 36 wt% after 30 min from introducing the feed to the reactor at the temperatures of 230 °C for F21 compared to 46 wt% for USY-C before the modification, and then decreasing with the TOS to 32 wt% after 1,000 min compared to 43 wt% after the same period of time, and decreasing slowly within the deactivation rate ranging between 1 and 3 wt% every 24 h until the reaction was terminated after almost 4 days. Figure 13b shows that the initial selectivity towards the hydroisomerisation products was 99 % for F21, which was the same as USY-C before the modification, and kept almost same along the deactivation run. As shown in Fig. 13c and d, the selectivity towards cracked and cyclic products was fairly similar for F21 compared with USY-C.

The influence of nickel on the stability of Pt/350HOA USY in the hydroisomerisation of n-C7

The catalytic properties of a bifunctional catalyst depend on the balance between its acidity and its hydrogenating functions. With respect to its selectivity and stability, increasing the proportion of the hydrogenation function at constant acidity leads to an improved catalyst performance, and for this reason, a series of monometallic and bimetallic bifunctional catalysts was formed by loading the H-USY (350HOA USY, with a global Si/Al = 5 mol/mol, supplied by Tosoh Corporation) with different amounts of platinum, nickel and platinum–nickel by competitive ion exchange, then investigating the effects of nickel as a second metal to Pt on the stability of the Pt/350HOA USY catalyst in the hydroisomerisation of n-C7 at 230 °C and 1 atm using H_2/C7 = 9 and WHSV = 5.13 h^{-1}. The first series comprised monometallic bifunctional catalysts containing 0.5, 1, 1.5 and 2 wt% of platinum supported on H-USY (350HOA USY), the second was a series of monometallic bifunctional catalysts containing 0.5, 1, 1.5, 2, 10 and 20 wt% of nickel, also supported on 350HOA USY, and the third series was of bimetallic bifunctional catalysts containing 1 wt% of platinum and 0.25, 0.5, 0.75 and 1 wt% of nickel, again supported on 350HOA USY. The monometallic catalysts were prepared using the ion-exchange method, while the method used for the bimetallic catalysts was simultaneous competitive ion exchange, which means that the platinum and nickel precursors, $Pt(NH_3)_4Cl_2H_2O$ and $Ni(NO_3)_26H_2O$, respectively, were mixed together with the zeolite, at the liquid-to-solid ratio of 50 (1 g of zeolite to 50 ml of the metal complex solution), using ammonium hydroxide solution to adjust the pH of the suspension obtained at >9 in order to enhance the uptake and homogenous distribution of the metals within the zeolite grain.

Table 10 shows some characteristics of the mono- and bimetallic bifunctional catalysts so formulated using characterisation techniques such as ICP, XRD, NMR and TGA. Some results were also obtained using XPS and TEM. The quantitative uptake of the loaded metals was verified by elemental analysis using inductively coupled plasma spectroscopy for the hydrofluoric acid digested zeolite samples. It was observed that the uptake of metals by the zeolite support was less than the calculated value. It has been reported that the USY zeolite in its ammonium form had greater ion-exchange efficiency than the zeolite H-USY, due to the greater reduction in the pH of the reaction medium in the latter case [40]. The pH was adjusted for this reason, even though the desired molar ratio for the bimetallic catalyst Pt–Ni/USY was obtained. Using X-ray diffraction, it was found that all the diffraction patterns of the metal-loaded catalysts were identical to that of the parent sample of 350HOA USY. Moreover, no

Table 9 In-house characterisation of original catalysts and those modified by AHFS

	AHFSwt (g)	USYwt (g)	Mixing time (h)	Temp (°C)	Vol (ml)	Si (wt%)	Al (wt%)	F (wt%)	Pt (wt%)	Bulk Si/Al, molar ratio	Framework Si/Al, molar ratio	Crystal (%)	NH_3 TPD (mmol g^{-1})	(Si/Al), Atomic Conc %(XPS)	Pt, Atomic conc % (XPS)	Surface area (m^2/g)	Pore volume (cm^3/g)	Pore size (Å)
320USY	–	–	–	–	–	29.36	9.73	–	0.83	2.90	6.41	63.68	0.3	2.24	0	735.87	0.39	34.52
F2	0.6	2	1	25	50	30.71	5.22	0.56	0.94	5.65	6.45	57.27	1.05	5.32	0	818.98	0.45	31.43
USY-A	–	–	–	–	–	26.75	9.71	–	1.01	2.87	7.11	99.16	0.86	2.22	0.03	755.67	0.42	27.99
F20	0.6	2	1	25	50	33.57	4.53	0.03	0.87	7.12	9.51	70.17	1.11	10.23	0.03	774.25	0.42	26.66
USY-C	–	–	–	–	–	28.51	9.80	–	0.99	2.79	7.84	98.35	0.60	1.25	0.03	519.16	0.37	41.84
F21	0.6	2	1	25	50	35.84	4.81	0.05	0.86	7.16	11.93	63.38	1.50	3.36	0	720.30	0.43	28.78
350USY	–	–	–	–	–	34.04	5.89	–	0.90	5.55	12.38	66.39	0.76	4.98	0.07	872.97	0.47	26.10
F22	0.6	2	1	25	50	39.39	1.06	0.05	0.84	36.19	13.69	72.58	0.49	16.16	0	917.30	0.46	22.12

diffraction peaks were assigned to Pt or Ni, which may indicate high dispersion of these metals. The crystallinity results obtained were in the range of 60–78, versus 66 % for the parent material. The TEM images for the 1 wt% Pt–1 wt% Ni, 2 wt% Pt and spent 2 wt% Pt/350USY catalysts are shown in Fig. 14. The black dots appearing on the support matrix are assumed to be Pt or Pt–Ni particles. The average size of the visible metal particles was found to be in the range of 3–7 nm for the Pt–Ni bimetallic catalyst and in the range of 3–30 nm for the monometallic samples, as measured manually and averaged [41], indicating that the presence of nickel and platinum in the bimetallic catalysts enhanced greatly the formation of metal particles and reduced their sizes. It was also found that the presence of platinum improved the nickel reduction in comparison to the presence of nickel only [40]. As in the faujasite zeolite structure (zeolite Y), the cavities had a maximum diameter of 1.3 nm, which means that the observed metal particles were located outside the zeolite cavities. Nevertheless, these metallic particles could have been located within the mesopore channels which were created during the hydrothermal dealumination of the Y zeolite, or at the outer surface of the catalyst grains, as has been reported [40]. It has also been suggested that there are likely to be smaller metal particles inside the cavities which are not detectable by TEM [42, 43]. It was observed that the average metallic particle size in the case of the 2 wt% Pt/350USY was unchanged by the deactivation reaction, which may indicate that no metal sintering occurred; however, this conclusion cannot be assured, as TEM was able to study only limited regions of the samples and consequently the results should be interpreted as mainly local [43].

The Figs. 15, 16, and 17 show the effect of TOS on the n-C7 conversion, hydroisomerisation, hydrocracking and cyclic product yields at the reaction temperature of 230 °C for the first, second and third series of monometallic and bimetallic bifunctional catalysts containing platinum and nickel, supported on H-USY (350HOA USY). Figure 15a indicates that the initial overall conversion values were 47, 56, 57, and 51 wt% for the monometallic catalysts containing Pt of 0.5, 1, 1.5, and 2 wt%, respectively, after 30 min from introducing the feed to the reactor at the temperature of 230 °C. All the catalysts underwent small decreases in conversion with TOS up to 12 h, after which there was a significant decrease in conversion for the catalyst containing 0.5 wt% Pt. The catalyst containing 2 wt% Pt was found to have the smaller drop in conversion, while that containing 0.5 wt% Pt underwent greatest fall in activity during the TOS. The higher sustainability of the catalyst containing 2 wt% Pt can be explained by the formation of catalytically active metallic particles and better balance between metal and acid sites, as shown in Table 10.

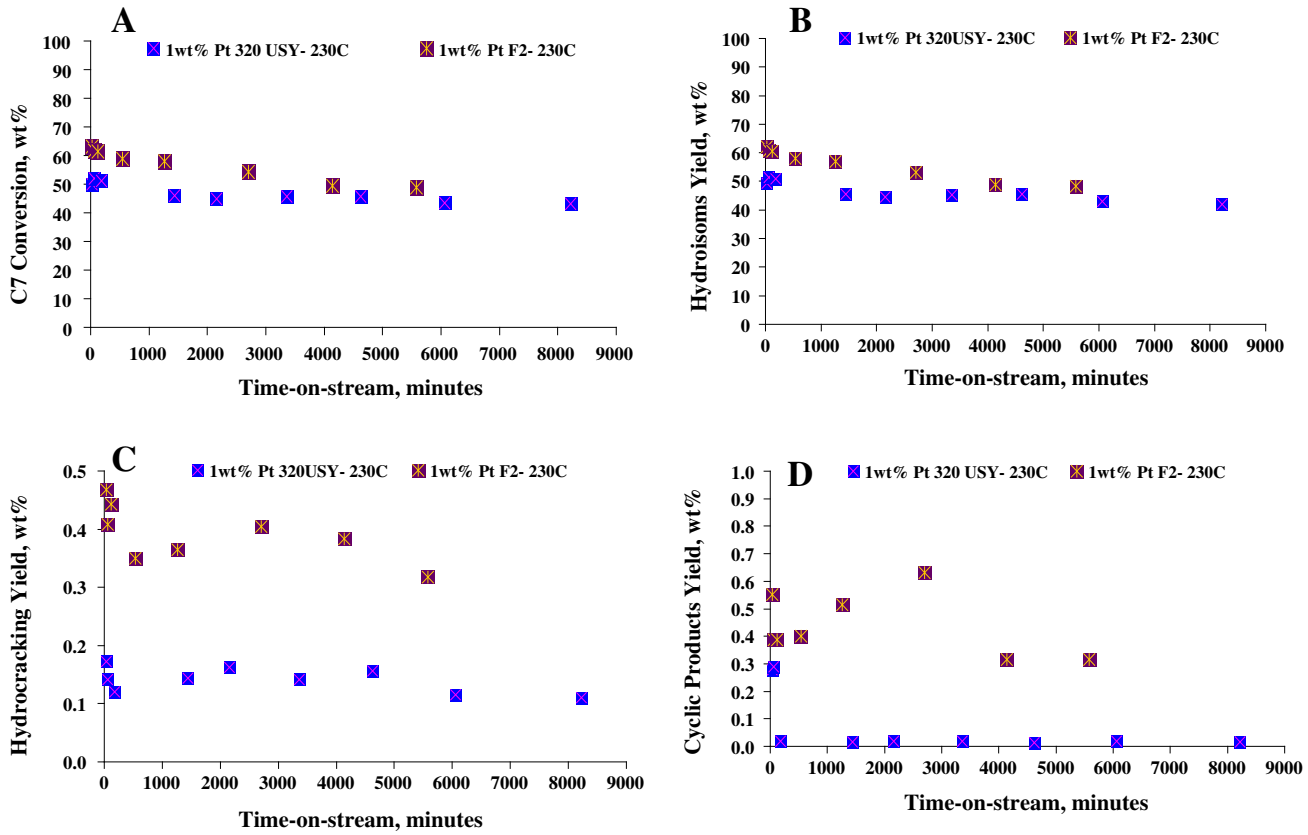

Fig. 11 Overall conversion (**a**), total yield of C7 isomers (mono + di + tribranched isomers) (**b**), total hydrocracking yield (**c**), and total yield of the cyclic products (**d**) as a function of TOS for F2 catalyst at various reaction temperatures. WHSV = 5.13 h^{-1}; H_2/C7 (mol/mol) = 9; total pressure = 1 atm; temperature = 230 °C; 1 wt% Pt loading

Figure 15b shows that the initial selectivity towards the hydroisomerisation products ranged between 98 and 99 % for all the catalysts, remaining almost unchanged throughout the deactivation run. Furthermore, as shown in the Fig. 15c and d, the selectivity towards cracked and cyclic products respectively was fairly in the range of 1 and 2 % for all the catalysts even if their n_{Pt}/n_A ratio is quite different. Nevertheless, n_{Pt}/n_A ratio was found to be within the optimum balance limits of 0.03 and 0.17 ($0.03 \leq n_{Pt}/n_A \leq 0.17$) for the most catalysts, which may reflect the great dehydrogenation–hydrogenation function capacity of platinum even at the lower contents [40, 41, 44]. The average hard coke contents were found to be in the range of 0.1–0.2 wt% for all the catalysts except that containing 1 wt% platinum, for which the coke content was about 0.7 wt%, which may due to the effect of the longer TOS when compared with the other catalysts.

Figure 16a shows that 30 min after introducing the feed into the reactor at 230 °C, the initial overall conversion rates were 52 and 59 wt%, respectively, for the monometallic catalysts containing 10 and 20 wt% Ni. After 180 min on stream, there was a large drop in activity to 30 and 45 wt%, then a sustained and rapid deactivation rate until a pseudo-stable state was reached at activity levels of 10 and 16 wt%, respectively, persisting until the reactions terminated. Deactivation was also found to be very rapid for the monometallic catalysts containing Ni at 0.5, 1, 1.5 and 2 wt%. This behaviour may be explained in terms of the poor hydrogenating capacity of Ni compared to Pt [44], making it more difficult for the Ni atoms to be fully reduced, so that not enough Ni metallic sites were available to sustain the reaction, since the hydroisomerisation reaction includes a dehydrogenation step [40, 42]. Therefore, selectivity to form the C7 isomers was lower than for the catalysts containing Pt, while higher cracked and cyclic product yields were obtained, which means that higher coke content was formed, possibly blocking and poisoning the active sites of the catalysts during the deactivation reaction. In addition, the low stability of catalysts with higher nickel content may be explained by the tendency of Ni to polymerise olefins and hence to form coke [42].

Figure 17a shows that the initial overall conversion rates were 66, 72, 66 and 67 wt% for the bimetallic bifunctional catalysts containing 1 wt% Pt and 0.25, 0.5, 0.75 and 1 wt% Ni, respectively, 30 min after introducing the feed into the reactor. All of these catalysts showed small decreases in conversion with TOS up to 12 h, after which there was a continuous moderate decrease in conversion

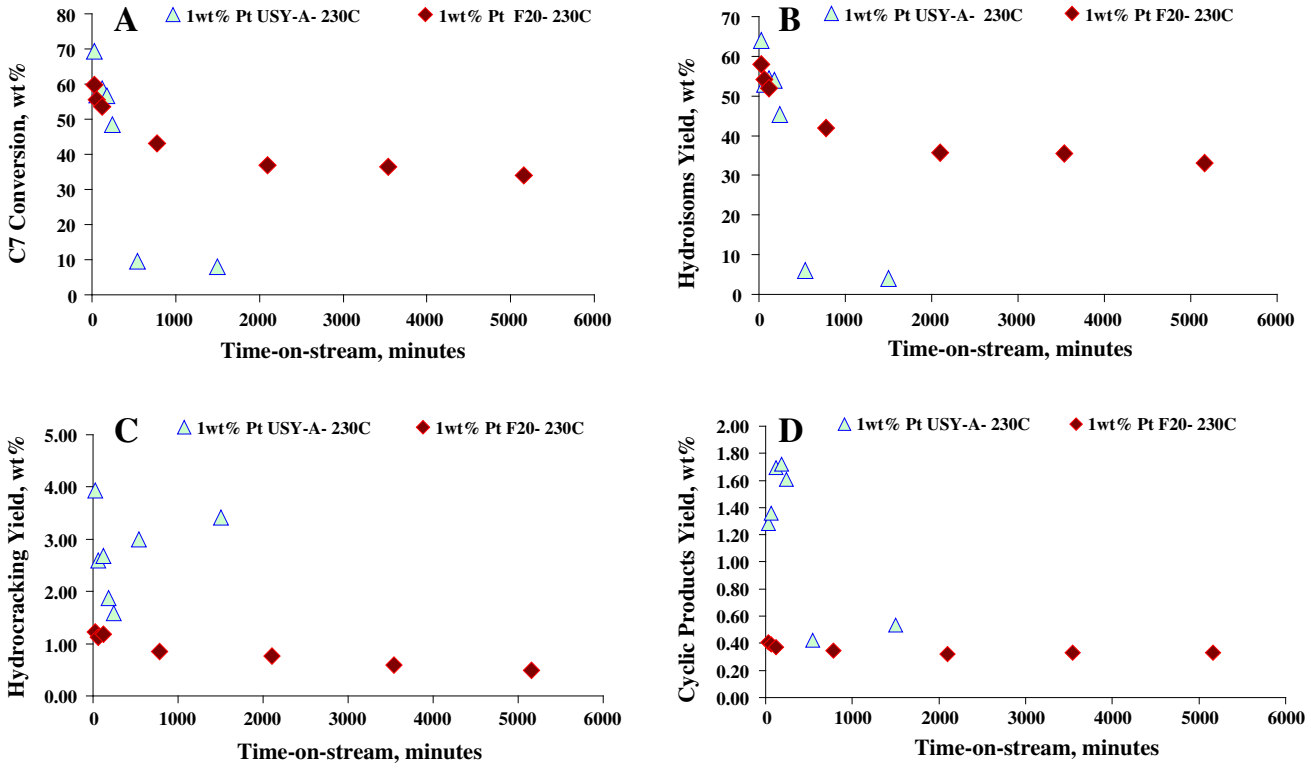

Fig. 12 Overall conversion (**a**), total yield of C7 isomers (mono + di + tribranched isomers) (**b**), total hydrocracking yield (**c**), and total yield of the cyclic products (**d**) as a function of TOS for F20 catalyst at various reaction temperatures. WHSV = 5.13 h^{-1}; H_2/C7 (mol/mol) = 9; total pressure = 1 atm; temperature = 230 °C; 1 wt% Pt loading

until the reactions terminated. Figure 17b indicates that initial selectivity towards the hydroisomerisation products ranged between 98 and 99 % for all of the catalysts, remaining almost constant throughout the deactivation run. Furthermore, as shown in the Fig. 17c and d, selectivity towards cracked and cyclic products respectively was broadly in the range of 1–2 % for all of the catalysts. On the other hand, the maximum hard coke content was found in the bimetallic catalyst containing 1 wt% Pt and 1 wt% Ni, as shown in the Table 10.

It can be concluded that a small addition of Pt motivated a substantial increase in hydrogenating activity when compared with the catalysts containing only Ni, as reported in the literature [30]. It also appears that the presence of platinum enhanced the reduction of the nickel cations, increasing the dispersion of the two metals as the nickel particles provided support for the Pt atoms, indicating that the Pt atoms were inserted into the nickel crystallite [40, 42]. On the other hand, it was found that increasing Ni loadings inhibited both the activity and selectivity of the catalyst, which may be interpreted as indicating that the formation of larger bimetallic Ni–Pt particles at higher Ni loadings resulted in some Ni content not being reduced, thus contributing to pore blockage of the catalyst and reducing the availability of catalyst acid sites accordingly [44].

Effect of platinum loading method on CP814E beta

Bifunctional zeolite catalysts typically have two types of active centres, the hydrogenation/dehydrogenation sites provided by the metal (such as platinum) for the formation of olefinic intermediates, and the acidic site for isomerisation and cracking. In the case of Pt-loaded zeolite catalysts in the ammonium form, the method most commonly used to introduce platinum into the pores and obtain a homogeneous filling in the crystallites of the zeolite is cationic exchange, using platinum tetraammine $[Pt(NH_3)_4]^{2+}$ complexes in an aqueous solution in the presence of a competing cation, generally an ammonium ion, NH_4^+. A second method to introduce platinum in the pores is incipient wetness impregnation by which the platinum tetraammine will randomly be deposited in the zeolite pores whereas only one platinum tetraammine complex can be associated with an aluminium site, and thus an atomic dispersion of the complexes inside the pores is expected with the ion-exchange method. Therefore, more dispersed platinum and consequently smaller particles using the ion-exchange method would be produced than via the impregnation method [27, 29, 45]. The purpose of this study was to examine the effects of platinum loading of beta zeolite by ion-exchange and impregnation methods, examining the

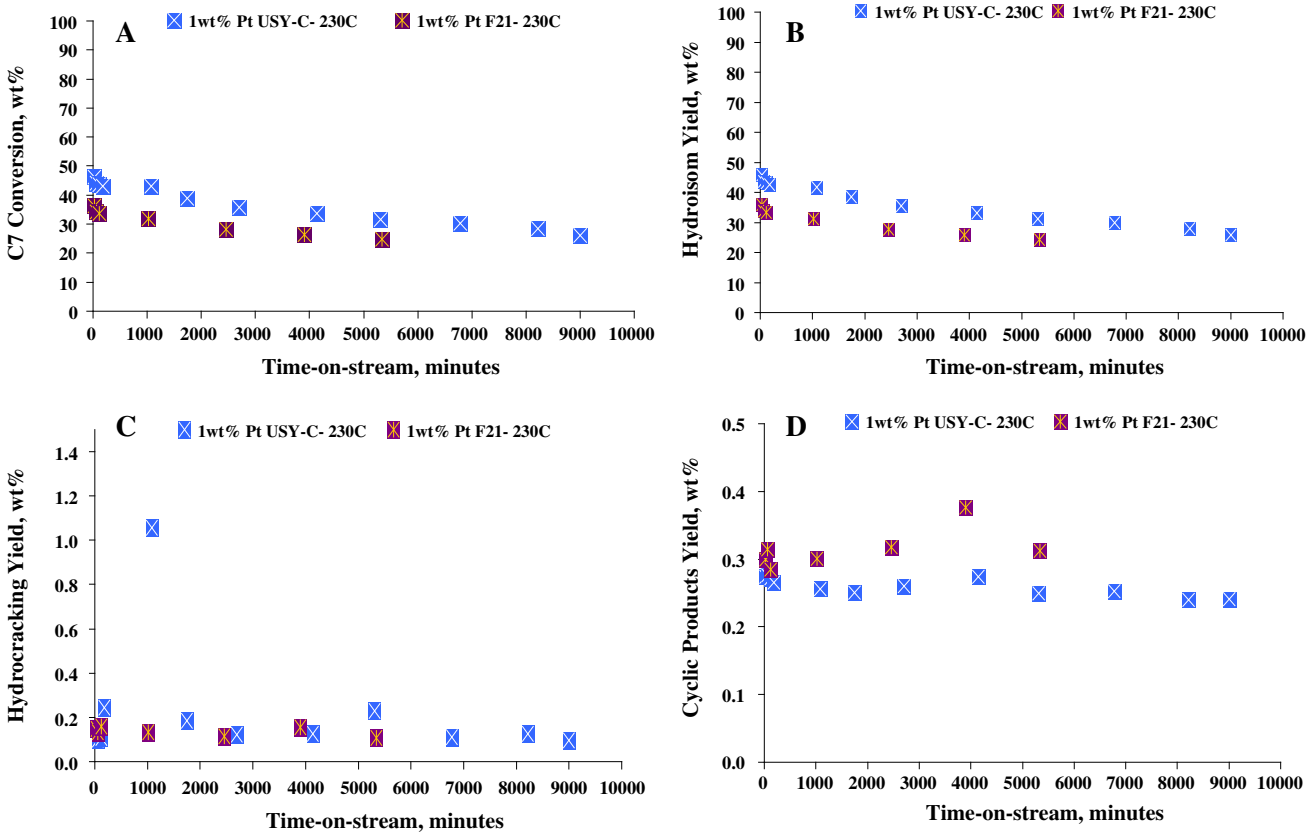

Fig. 13 Overall conversion (**a**), total yield of C7 isomers (mono + di + tribranched isomers) (**b**), total hydrocracking yield (**c**), and total yield of the cyclic products (**d**) as a function of TOS for F21 catalyst at various reaction temperatures. WHSV = 5.13 h^{-1}; H_2/C7 (mol/mol) = 9; total pressure = 1 atm; temperature = 230 °C; 1 wt% Pt loading

TOS stability of 1wt% Pt-loaded CP814 beta, where its deactivation behaviour was studied in the previous work [31], in the hydroisomerisation of n-C7 at constant reaction conditions and the effect of pH on the ion-exchange process.

Figure 18a–d shows the effects of TOS for the C7 conversion, hydroisomerisation, hydrocracking, and cyclic product yields for the catalyst with 1 wt% Pt/CP814E in which the platinum was loaded by one of three procedures: (1) preparation of the ion-exchange system using an aqueous solution of tetraammine platinum (II) chloride complex mixed with the ammonium-beta zeolite CP814E and the addition of the competing cation NH_4^+ using ammonia solution at pH > 9, (2) preparation of the ion-exchange system using an aqueous solution of tetraammine platinum (II) chloride complex mixed with the ammonium-beta zeolite CP814E without adding ammonia solution such that the pH = 4–5, and (3) preparation by wet impregnation using an aqueous solution of tetraammine platinum (II) chloride complex mixed with the ammonium-beta zeolite CP814E without adding ammonia solution, such that the pH = 4–5. As Fig. 18a shows, initially the overall conversion of C7 for the three catalysts was 77, 88, and 90 wt% after 30 min from the point when the feed was introduced to the reactor at 230 °C, prepared by the three procedures described above. The catalysts lost about 1–2 wt% of their activity before reaching a pseudo-stable state for the initial 60 min on stream, and then slightly decreased with a further increase in time until the reactions were finally terminated. On the other hand, the selectivity towards hydroisomerisation products was 99, 85, and 85 % after 30 min and then increased with time to 99, 89, and 89 % for the three catalysts, respectively. Furthermore, the greatest selectivity towards cracked products was 15 % and slightly decreased with TOS to approximately 9 % for the catalysts which were prepared by the ion-exchange method with pH = 4–5 and by the wet impregnation method. The selectivity towards the cyclic products was very low for the three catalysts along the deactivation runs.

The variation in C1/C3 mass ratio with TOS for the three catalysts at constant reaction conditions is shown in Fig. 19, with both the acid and metal functions being initially active and deactivated rapidly as indicated by the C1/C3 ratio. This could be explained by a change occurring in the balance between the two functions with TOS due to coke depositions for both functions. Furthermore, in all the

Table 10 Different metal loadings wt% on 350HOA USY

	Al (wt%)	Si (wt%)	Bulk (Si/Al) (mol/mol)	Framework (Si/Al) (mol/mol)	Crystallinity (%)	Actual Ni (wt%)	Actual Pt (wt%)	Theoretical Ni (wt%)	Theoretical Pt (wt%)	Ni/Pt (mol/mol)	n_{Pt}/n_A	Hard coke (wt%)
350HOA USY	5.89	34.04	5.55	12.38	66	–	–	–	–	–	–	–
Pt/350HOA USY												
0.5 %Pt	–	–	–	–	–	–	0.36	–	0.50	–	0.02	0.19
1 %Pt	5.89	34.04	5.55	12.38	66	–	0.90	–	1.00	–	0.06	0.66
1.5 % Pt	–	–	–	–	–	–	1.17	–	1.50	–	0.08	0.13
2 % Pt	–	–	–	–	–	–	1.46	–	2.00	–	0.10	0.14
Pt-Ni/350HOA USY												
1 % Pt–0.25 %Ni	5.29	27.50	5.00	–	60	0.22	0.90	0.25	1.00	0.81	0.11	0.47
1 % Pt–0.5 % Ni	5.29	27.60	5.01	–	63	0.44	0.91	0.50	1.00	1.61	0.16	0.62
1 % Pt–0.75 %	5.31	27.65	5.00	–	61	0.68	0.92	0.75	1.00	2.46	0.21	0.43
1 % Pt–1 % Ni	5.31	27.97	5.06	11.57	60	0.92	0.91	1.00	1.00	3.36	0.27	1.01
Ni/350HOA USY												
0.5 % Ni	–	–	–	–	–	0.44	–	0.50	–	–	0.10	–
1 % Ni	–	–	–	–	–	0.88	–	1.00	–	–	0.20	–
1.5 % Ni	–	–	–	–	–	1.28	–	1.50	–	–	0.29	–
2 % Ni	–	–	–	11.03	–	1.86	–	2.00	–	–	0.42	–
10 % Ni	4.74	27.74	5.62	10.86	73	7.48	–	10.00	–	–	1.68	–
20 % Ni	4.28	24.83	5.57	10.58	–	11.96	–	20.00	–	–	2.68	–

three catalysts, the metal function deactivated faster than the acid function; however, this was not severe enough to cause a drop in the n-C7 conversion. The worst metal/acid balance was found for the catalysts that were prepared by ion exchange with the pH = 4–5 and by the wet impregnation method, as indicated by the lower values of C1/C3, and as such higher cracking activity was observed for those two catalysts. Moreover, the two catalysts demonstrated poor metal dispersion resulting in some of the metal being deposited on the outside of the crystals and not within the zeolite pores, as compared to the catalyst that was prepared by ion exchange with the pH > 9.

Effect of CP814E composites

The zeolite-based composite materials consisting of two distinct phases with entirely different pore structure and acidity have been used extensively both as catalysts, and to minimise the formation of coking, thus increasing the lifetime of the catalyst. Beta zeolite can also be used as an additive to FCC cracking catalysts because it favours reactions that improve the octane number of gasoline since the feedstocks consist of bulky poly-nuclear molecules which cannot diffuse inside the zeolite pores. Composite catalysts made of a zeolitic and a non-zeolitic active oxide/poly-oxide as a matrix can be used to crack the bulky feed molecules into smaller molecules which can diffuse inside the zeolite pores providing a two-phase system of the composite that operates synergistically. This synergism is a result of the open structure of the matrix that allows easy intra-particle diffusion and favours the primary cracking of the bulky feed molecules, as a result of the balance between the acidic sites and the metallic sites due to the dispersion of Pt throughout the matrix [27, 46, 47].

In this work, TOS experiments were carried out on the hydroisomerisation of n-C7 using hybrid catalysts consisting of CP814E and USY-C at identical reaction conditions, and thus the relation between zeolite pore structure and its resistance to coke deactivation is examined for the composite catalysts formed. Two composite bifunctional catalysts were prepared as follows: (1) the catalysts 1 wt% Pt/CP814E and 1 wt% Pt/USY-C were mixed physically at mass ratio of 1:1. (2) CP814E and USY-C in their ammonium forms were mixed at mass ratio of 1:1, and were loaded by 1 wt% Pt using the ion-exchange method.

The effect of TOS on the C7 conversion, hydroisomerisation, hydrocracking, and cyclic product yields at reaction temperature of 230 °C are shown in the Fig. 20a–d,

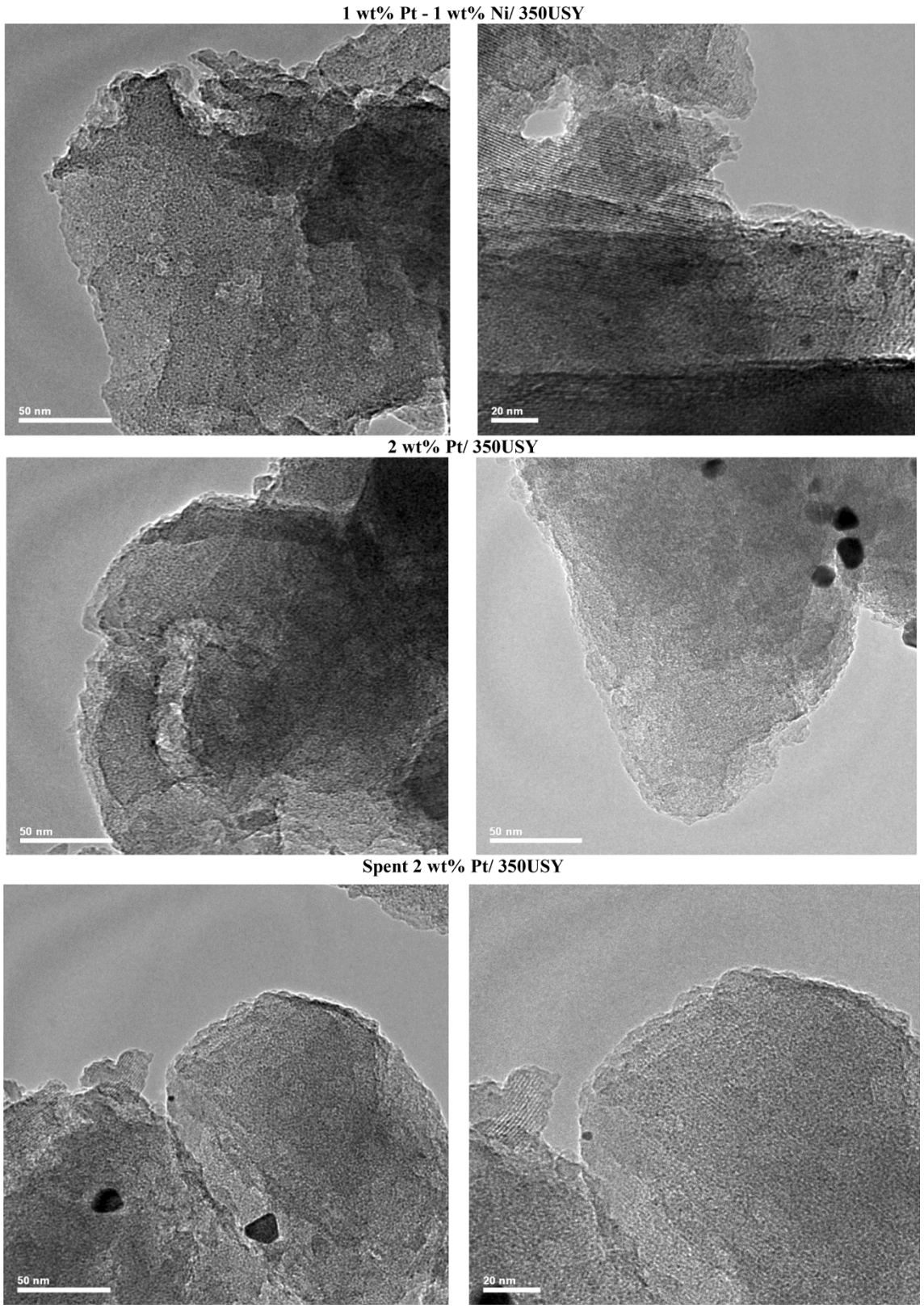

Fig. 14 TEM images of 1 wt% Pt–1wt% Ni, 2 wt% Pt and spent 2 wt% Pt/350USY

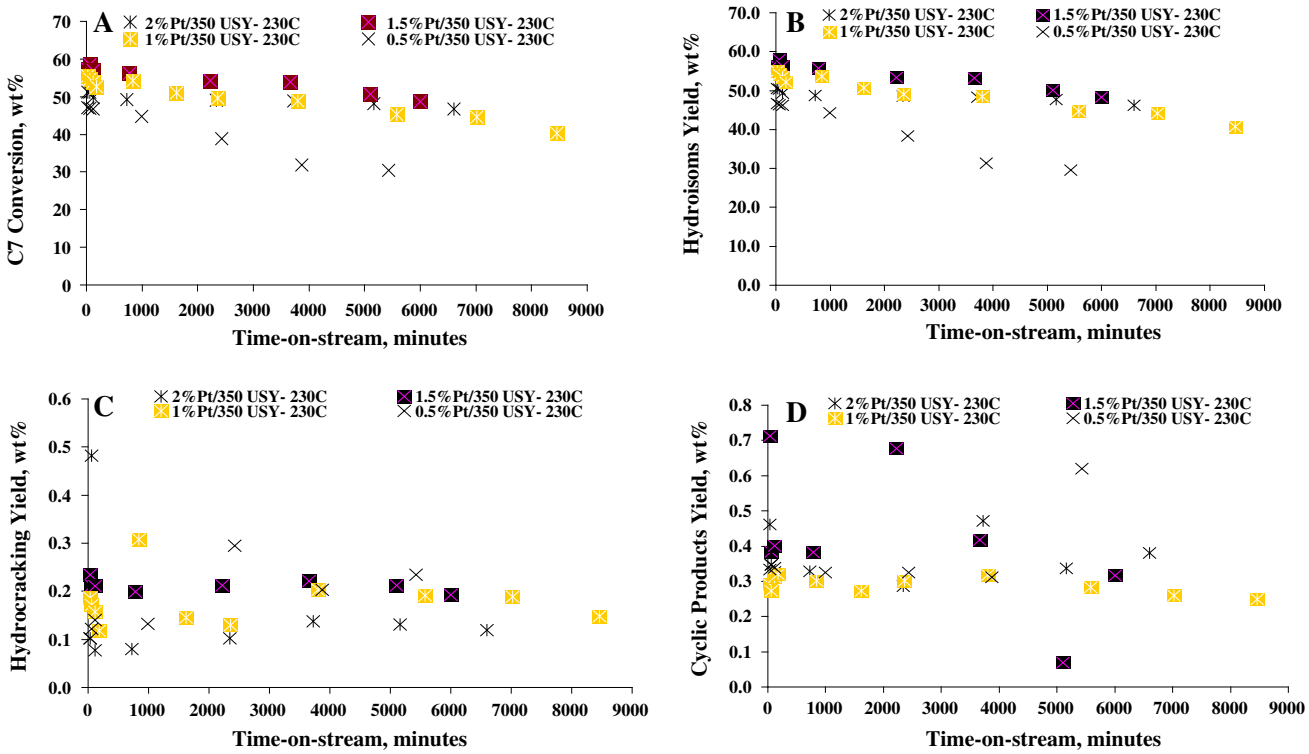

Fig. 15 Overall conversion (**a**), total yield of C7 isomers (mono + di + tribranched isomers) (**b**), total hydrocracking yield (**c**), and total yield of the cyclic products (**d**) as a function of TOS for the monometallic catalysts containing Pt at various reaction temperatures. WHSV = 5.13 h^{-1}; H_2/C7 (mol/mol) = 9; total pressure = 1 atm; temperature = 230 °C; 1 wt% Pt loading

respectively, for the catalysts: 1 wt% Pt/CP814E, 1 wt% Pt/USY-C, 1 wt% Pt/USY-CP814E physically mixed, and 1 wt% Pt/USY-CP814E physically mixed and loaded by Pt together by the ion-exchange method with ammonia added to adjust the pH to be more than 9. As Fig. 20a shows, initially the overall conversion of C7 for the 1 wt% Pt/USY-CP814E physically mixed was 66 wt%, which is in between that of the corresponding individual catalysts, compared with 77 and 46 wt% for the catalysts 1 wt% Pt/CP814E and 1 wt% Pt/USY-C, respectively. The conversion then decreased abruptly at the initial stages of the reaction, and finally reached a relatively steady value, after which the conversion decreased steeply with the TOS until the reaction was terminated after 183 h. Thus, this composite catalyst demonstrated a better TOS activity than 1 wt% Pt/USY-C catalyst, but slightly worse than 1 wt% Pt/CP814E. Even its selectivity toward the C7 isomers and cracked products was very similar to both catalysts along the deactivation run.

On the other hand, the composite catalyst 1 wt% Pt/USY-CP814E, physically mixed and loaded with Pt using ion exchange and subsequently deactivated as with the 1 wt% Pt/CP814E catalyst, offered slightly higher activity towards the cracked products along the deactivation run, with the initial conversion of 78 wt% decreasing slightly with TOS to 67 wt% with the reaction terminating after 83 h. The selectivity towards the C7 isomers and cracked products was 96 and 3 %, respectively, and the composite catalyst demonstrated a better TOS activity than the 1 wt% Pt/USY-C catalyst, and a similar deactivation pattern to the 1 wt% Pt/CP814E even though the selectivity towards the cracked products was higher. This indicates that the 1 wt% Pt/USY-C catalyst was the dominant component in the formulated composite catalyst of 1 wt% Pt/USY-CP814E and provided a better TOS stability and higher activity. On the other hand, the 1 wt% Pt/CP814E catalyst was the dominant component for the composite catalyst 1 wt% Pt/USY-CP814E loaded with Pt using ion exchange. Figure 21 shows the deposited hard coke contents over the top, middle, and bottom zones of the individual and composite catalysts. It can be seen that the lowest hard coke content was found for the 1 wt% Pt/USY-C and the highest for the 1 wt% Pt/CP814E catalyst, with the composite catalyst having a hard coke content part way between that of the corresponding individual catalysts. The total acidity for ammonia TPD for the 1 wt% Pt/CP814E, 1 wt% Pt/USY-C, and 1 wt% Pt/USY-CP814E physically mixed was found to be 0.63, 0.60 and 1.88 mmol g^{-1}, respectively. Thus, it can be seen that even the composite catalyst has the highest acidity which is almost double compared with the corresponding individual catalysts. It has moderate hard coke content and fairly good TOS catalytic stability.

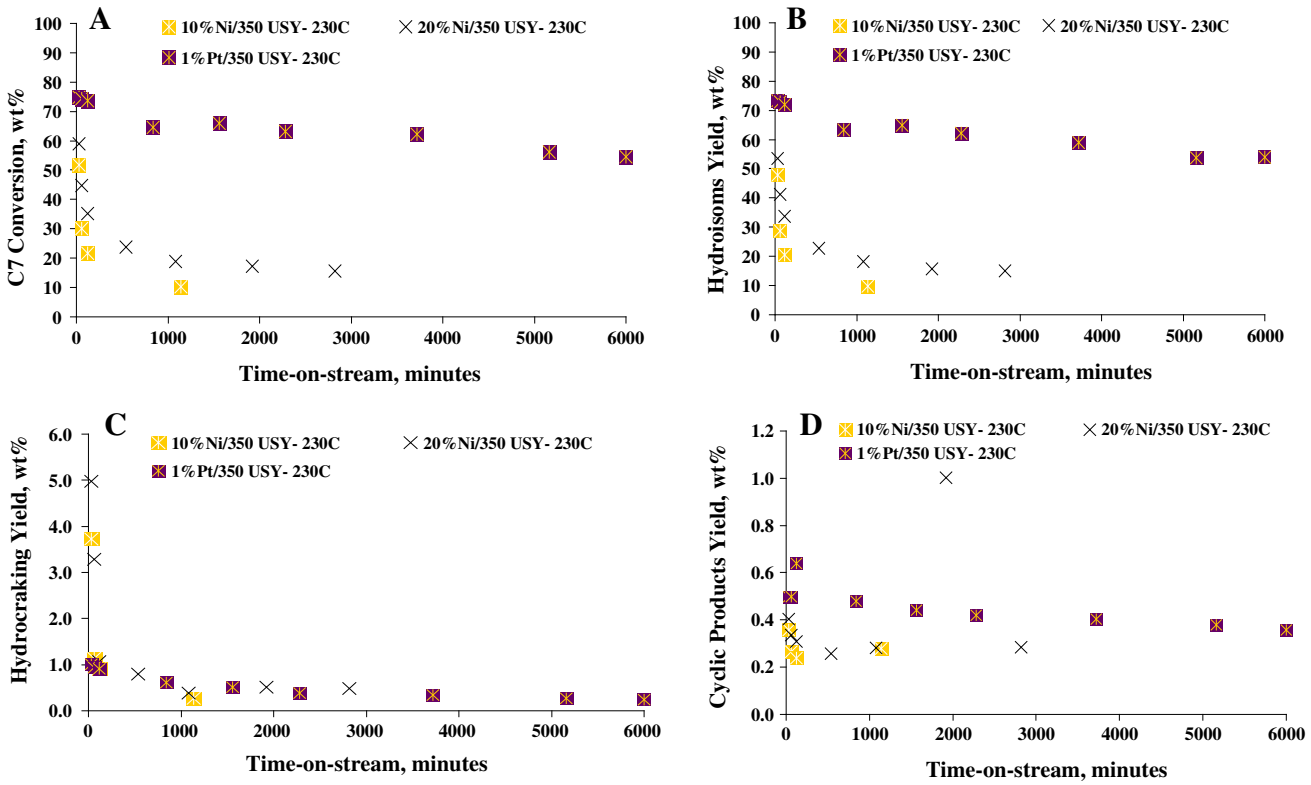

Fig. 16 Overall conversion (**a**), total yield of C7 isomers (mono + di + tribranched isomers) (**b**), total hydrocracking yield (**c**), and total yield of the cyclic products (**d**) as a function of TOS for the monometallic catalysts containing Ni at different reaction temperatures. WHSV = 5.13 h^{-1}; H_2/C7 (mol/mol) = 9; total pressure = 1 atm; temperature = 230 °C; 1 wt% Pt loading

Main characteristics of in-house mordenite zeolites

Mordenite zeolite was synthesised using the molar gel composition of (6 Na_2O: Al_2O_3: 30 SiO_2: 780 H_2O), which is the synthesis recipe of mordenite obtained from a verified synthesis handbook [21]. The mordenite phase with the highest purity and crystallinity was optimised against certain synthesis parameters while keeping this composition ratio constant. Three factors were optimised: the ageing time of the synthesis gel, the crystallisation time and the crystallisation temperature. Table 11 shows the phase crystallinity, the bulk Si/Al ratio and the framework Si/Al ratio of the mordenite obtained by optimising these three factors. It can be seen that the optimum synthesis conditions were when the ageing time was 12 h, crystallisation time was 24 h and crystallisation temperature was 180 °C. Under these conditions, the mordenite zeolite phase obtained had a crystallinity of 82 %, bulk Si/Al ratio of 8.44 (mol/mol) and framework Si/Al ratio of 9.02 (mol/mol). This procedure was repeated more than 10 times and reproducible results were obtained in terms of the yield, crystallinity, bulk and framework Si/Al ratio, as well as of the crystal morphology and size.

Figures 22 and 23 show the SEM microgram and XRD pattern of this in-house mordenite catalyst. The former shows that the catalyst contained large crystallites of 15–20 μm whose elliptical shape was different from that of commercial catalysts, and it has been previously reported that synthetic mordenite presents several morphologies, as a function of the crystallisation conditions [48]. The XRD patterns show a pure phase of mordenite consistent with that found previously [49]. However, it had a lower crystallinity than CBV21A [31], which also has a higher bulk Si/Al ratio. Figure 24a and b shows respectively the ^{27}Al and ^{29}Si solid-state NMR spectra of this in-house mordenite catalyst. It can be seen that the catalyst had only one ^{27}Al peak at about 56 ppm, which was assigned to tetrahedrally coordinated aluminium, and there were no additional EFAL peaks. In the ^{29}Si MAS NMR spectrum, two peaks at 112 and 106 ppm were assigned to Si(0Al) and Si(1Al) configurations, respectively.

Post-synthesis modification of in-house mordenite zeolite

Post-synthesis treatment by steam or acid attack, often referred to as dealumination, can remove aluminium from the zeolite framework. Steaming, which is performed at temperatures above 450 °C, extracts aluminium atoms from the framework and deposits them on the external

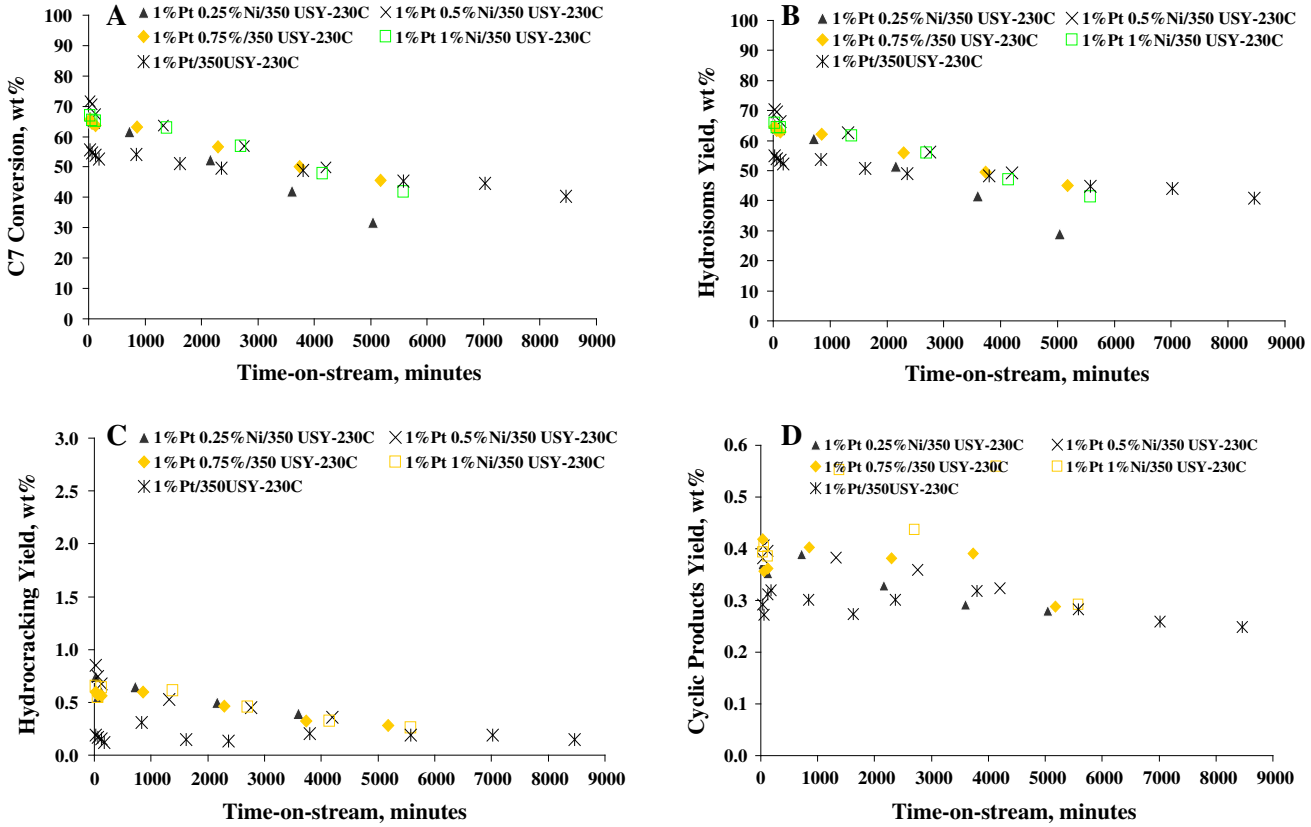

Fig. 17 Overall conversion (**a**), total yield of C7 isomers (mono + di + tribranched isomers) (**b**), total hydrocracking yield (**c**), and total yield of the cyclic products (**d**) as a function of TOS for the bimetallic catalysts containing Pt–Ni at different reaction temperatures. WHSV = 5.13 h^{-1}; H_2/C7 (mol/mol) = 9; total pressure = 1 atm; temperature = 230 °C; 1 wt% Pt loading

surface of the zeolite. An additional acid treatment can also be employed to completely remove aluminium atoms from the zeolite pore system. Increasing the framework Si/Al ratio by reducing the aluminium content in this way can result in the isolation of the remaining aluminium atoms, which in turn increases the strength of the acid sites and decreases the total number of active sites. This serves to improve both thermal and hydrothermal stability, while also generating mesopores, thus making the crystallite more accessible and reducing the severity of the diffusion limitations. Shortening the diffusion path length is of paramount importance for increasing the activity and stability of mordenite, as it is a one-dimensional, non-mesoporous zeolite. A small number of blockages can deactivate large parts of the mordenite structure [18, 50–52].

Two series of dealuminated mordenite catalysts were prepared by acid leaching and steaming applied to the in-house synthesised mordenite in its ammonium form. Table 12 shows the different acid leaching conditions that were applied to produce different catalysts with differing Si/Al ratios (acidity) based on the severity of acid leaching. In addition, three dealuminated mordenite catalysts were produced via the steaming dealumination technique at temperatures of 500, 600 and 700 °C. Table 13 shows the main characteristics of the acid-leached and steamed catalysts.

From Tables 5 and 6, it can be seen that the highest Si/Al molar ratios obtained for the framework and bulk were 19.13 and 42.76 (mol/mol), respectively, by acid leaching using nitric acid at a concentration of 10 molar, a temperature of 120 °C and a leaching time of 87 h (3.6 days), as in condition 15 in Table 12. A similar Si/Al ratio for the framework was obtained by increasing the acid leaching time to 168 h (7 days) at the same mixing temperature, as in condition 16, the most severe that was applied. It is generally expected that the bulk Si/Al molar ratio should remain the same even after steaming modification and that the steamed mordenite should have the same bulk Si/Al molar ratio as synthesised mordenite, but the framework Si/Al molar ratio was higher and increased as the steaming temperature increased from 500 to 700 °C, as shown in Table 13, which means that the framework aluminium atoms were dealuminated by steam to become EFAL.

Figures 25 and 26 show the SEM micrograms of steamed mordenites and the XRD patterns of acid-leached and steamed mordenites, respectively. From the SEM images, it can be seen that the steamed catalysts contained

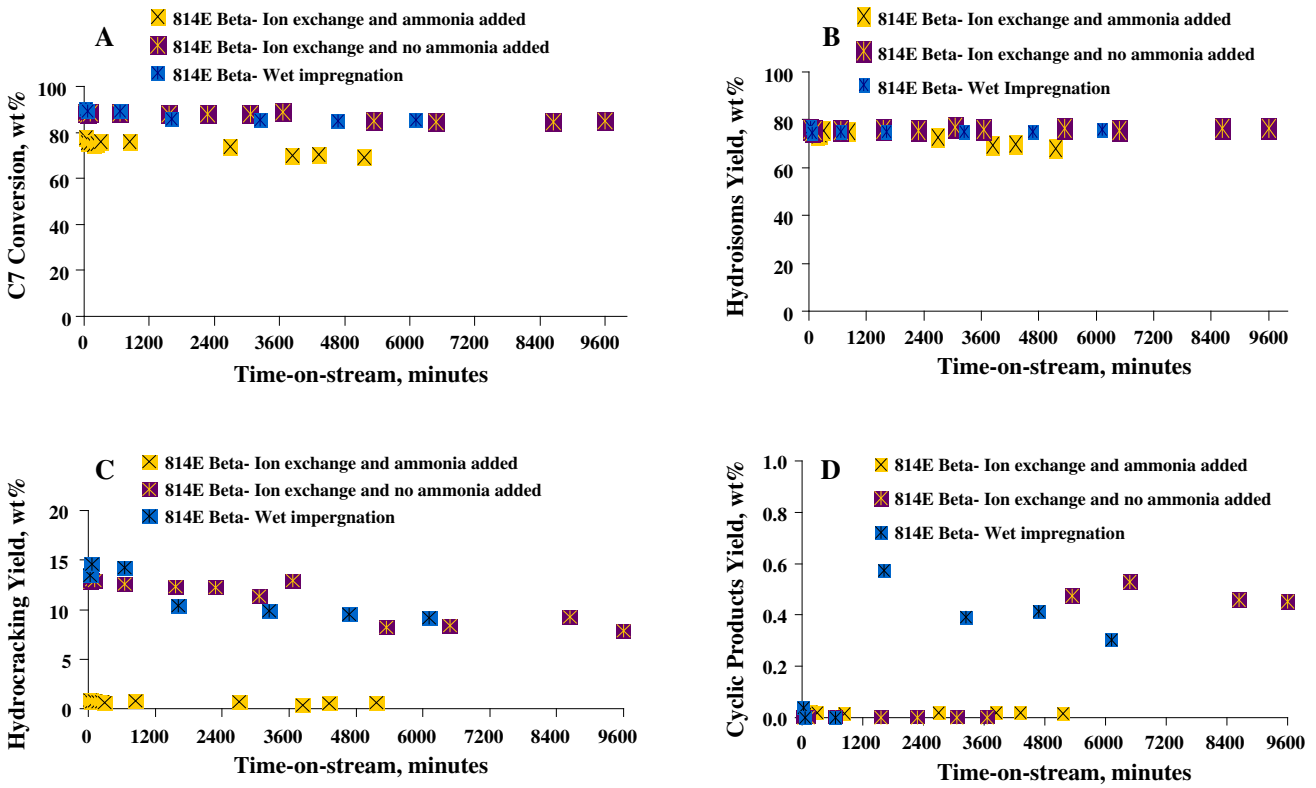

Fig. 18 Overall conversion (**a**), total yield of C7 isomers (mono + di + tribranched isomers) (**b**), total hydrocracking yield (**c**), and total yield of the cyclic products (**d**) as a function of TOS for CP814E. WHSV = 5.13 h^{-1}; H_2/C7 (mol/mol) = 9; total pressure = 1 atm; temperature = 230 °C; 1 wt% Pt loaded by different methods

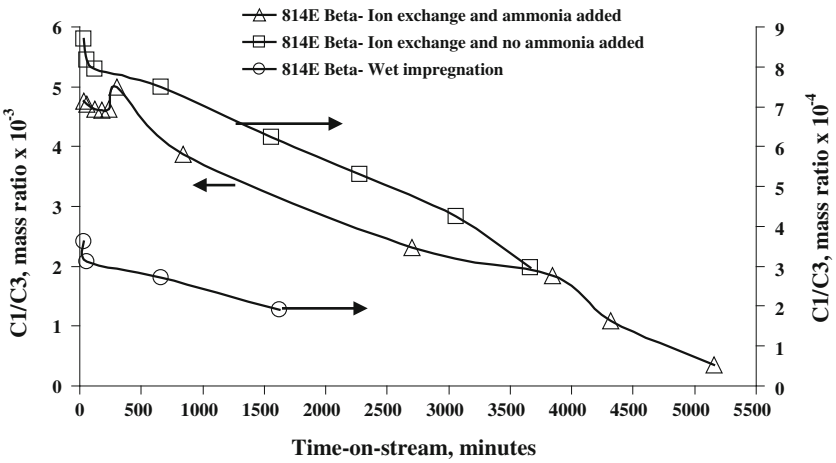

Fig. 19 Variation of the C1/C3 mass ratio as a function of TOS of CP814E

large and small crystallites of different sizes with some smaller debris and agglomerates whereas the acid-leached catalyst kept almost its original large crystal shape with some holes on the crystal surface. The XRD patterns confirm the pure mordenite phase for the steamed and acid-leached samples, with less overall crystallinity than as-synthesised mordenite.

Figures 27 and 28 show the ^{27}Al and ^{29}Si solid-state NMR spectra of acid-leached and steamed samples. It can be seen that the acid-leached catalysts had two ^{27}Al peaks, at about 56 and 0 ppm, assigned to a tetrahedrally coordinated aluminium atom in the framework and a smaller quantity of octahedrally coordinated aluminium as EFAL. Conversely, the steamed samples showed a very large quantity of EFAL at unique resonance spectra for octahedral and tetrahedral aluminium atoms at about 1 and 3 ppm, respectively, alongside in-framework aluminium in tetrahedral coordination. The quantity of EFAL also

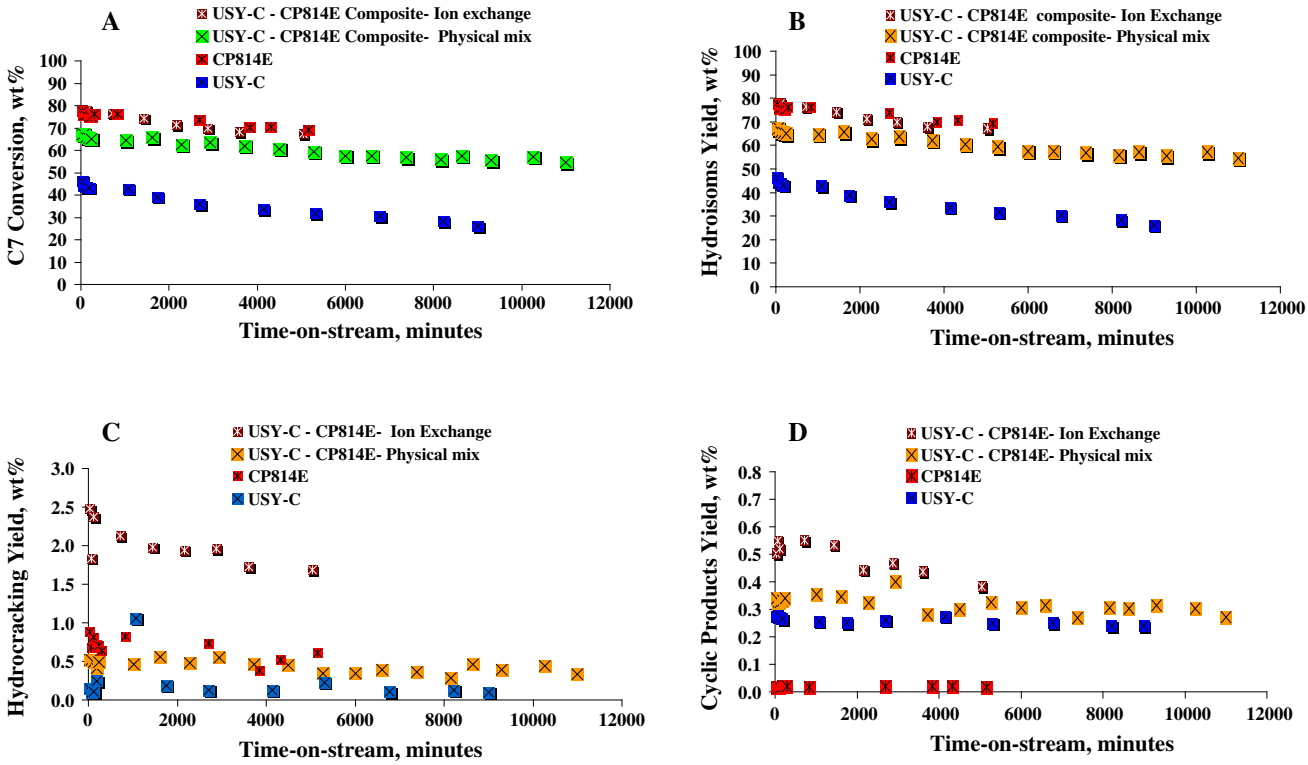

Fig. 20 Overall conversion (**a**), total yield of C7 isomers (mono + di + tribranched isomers) (**b**), total hydrocracking yield (**c**), and total yield of the cyclic products (**d**) as a function of TOS for USY and CP814E composites. WHSV = 5.13 h^{-1}; H_2/C7 (mol/mol) = 9; total pressure = 1 atm; temperature = 230 °C; 1 wt% Pt loading

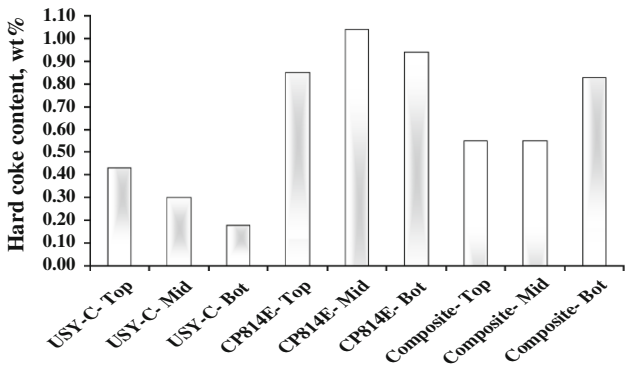

Fig. 21 The hard coke content over the aged CP814E, USY-C, and USY-CP814E physically mixed

increased as the steaming temperature increased. In the ^{29}Si MAS NMR spectra, two peaks at about 114 and 107 ppm were assigned respectively to Si(0Al) and Si(1Al) configurations, and these chemical shifts differ slightly from the sample produced by steaming. In addition, silicon atoms are different crystallographically as indicated by the different peak shape, depending upon the steaming temperature that was employed. However, the strong increase in the Si(0Al) signal intensity as the steaming temperature increased indicates that the replacement of Al by Si in the framework was more effective [20].

Table 13 and Fig. 29 show that the dealumination treatments by acid leaching and steaming resulted in an increase in mesoporosity, as illustrated with N_2-physisorption as a sharp increase in adsorption at high relative pressures, indicating the formation of large mesopores and a corresponding increase in the external surface area. Additionally, an average pore size of 27 Å was observed in the treated samples, compared with 18 Å for as-synthesised mordenite.

TOS behaviour during C7 hydroisomerisation conversion was examined for the following commercial and in-house mordenite catalysts: CBV10A, CBV21A, 640HOA, 660HOA, 690HOA [31], acid-leached mordenite and in-house mordenite steamed at 600 °C. All of the above catalysts were loaded with 1 wt% Pt by the ion-exchange method. Three very acidic commercial catalysts—1 wt% Pt/CBV10A, 1 wt% Pt/640HOA and 1 wt% Pt/660HOA—and the acid-leached mordenite deactivated very rapidly during the initial few seconds, due to a rapid coking that may have poisoned the acid sites of these catalysts and changed the effective acid site density needed for an ideal bifunctional conversion. As a consequence, no TOS results were reported for these catalysts. Figure 30a–d shows the effects of TOS at a reaction temperature of 230 °C on C7 conversion, hydroisomerisation, hydrocracking and cyclic

Table 11 In-house mordenite synthesis parameters and the resulting sample characteristics

Ageing time (h)	Crystallisation time (h)	Crystallisation temp (°C)	XRD crystallinity (%)	ICP Si/Al (mol/mol)	ICP Na (wt%)	NMR Si/Al (mol/mol)
1	1 day	180	43	9.50	3.63	8.03
3			64	9.70	3.99	9.13
4			75	8.36	3.26	8.97
6			77	8.13	3.15	8.97
8			75	7.83	3.08	8.98
10			75	7.92	3.07	8.98
12			82	8.44	3.14	9.02
15			80	7.99	3.23	8.97
24			49	8.92	3.09	8.62
12	12	180	Amorphous	–	–	–
	20		76	–	–	8.71
	22		75	–	–	8.89
	23		71	–	–	8.92
	24		82	8.44	3.14	9.02
	25		76	–	–	8.63
	26		72	–	–	8.63
	28		70	–	–	8.65
	36		Amorphous	–	–	–
12	1 day	170	Amorphous	–	–	–
		175	32	–	–	7.67
		180	82	8.44	3.14	9.02
		185	72	–	–	8.80
		190	71	–	–	8.63

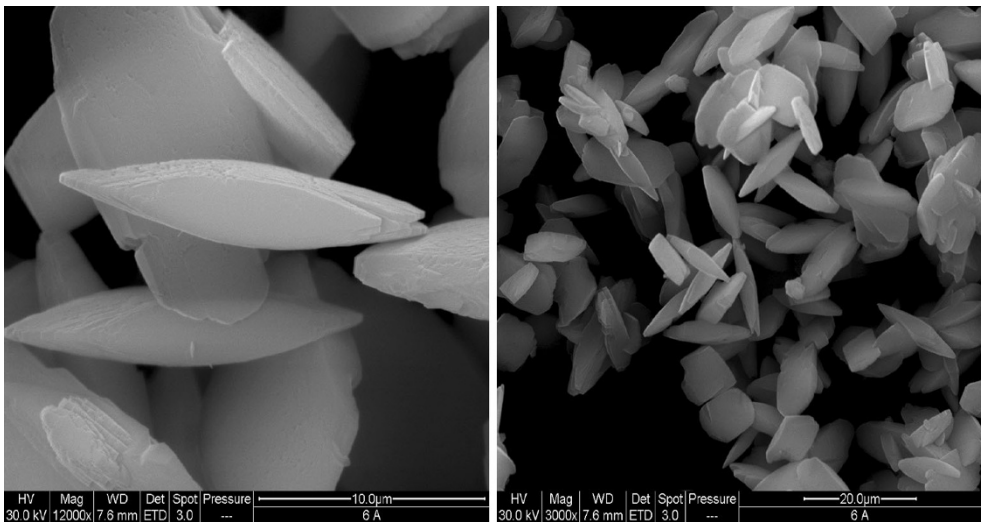

Fig. 22 SEM micrograph of in-house and as-synthesised mordenite

product yields respectively for the following catalysts: 1 wt% Pt/CBV21A, 1 wt% Pt/690HOA and in-house mordenite steamed at 600 °C.

Initially, the overall conversions were 12, 41 and 52 wt% after 60 min from the point when the feed was introduced to the reactor at 230 °C, for the 1 wt% Pt/CBV21A, 1 wt% Pt/690HOA and steamed mordenite catalysts, respectively. A rapid deactivation occurred for the 1 wt% Pt/CBV21A catalyst with high cracking activity, resulting in selectivity towards the cracked products at

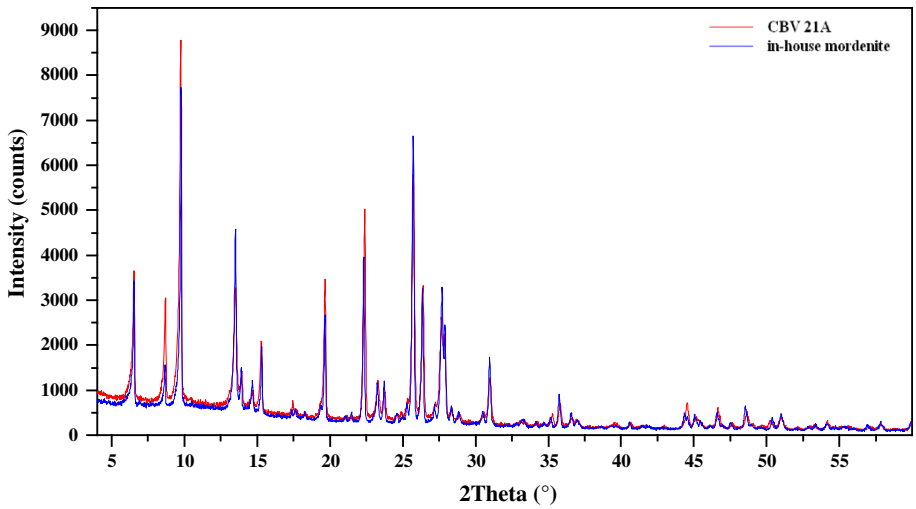

Fig. 23 XRD patterns of in-house and as-synthesised mordenite

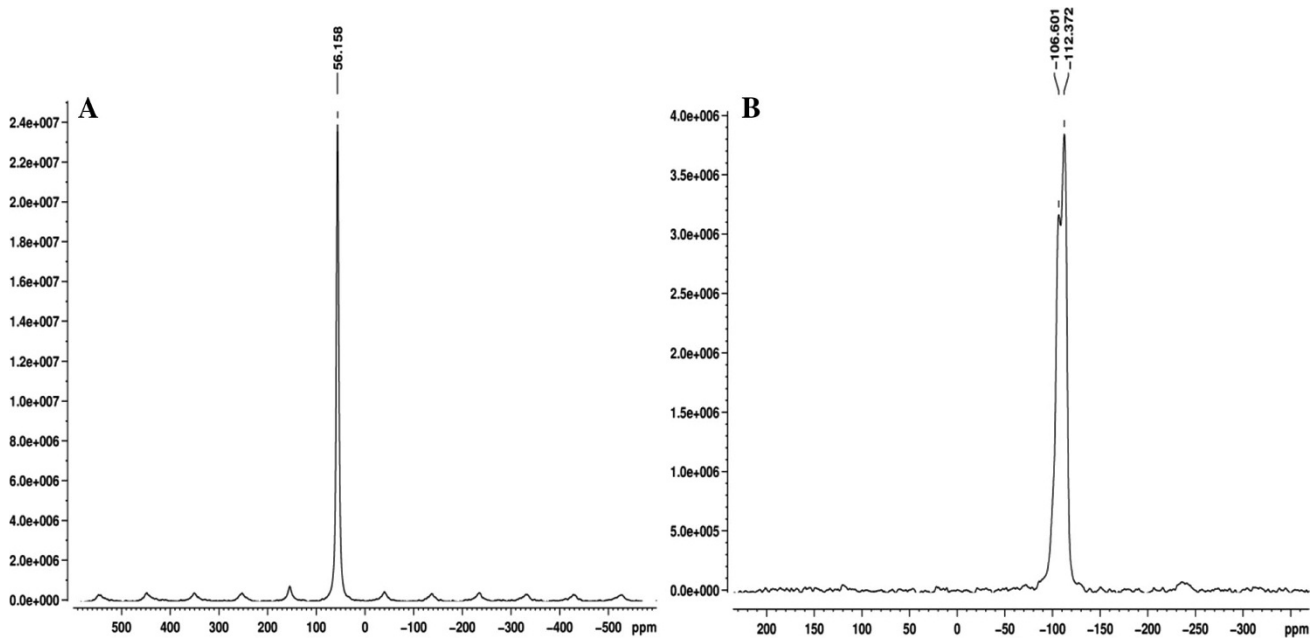

Fig. 24 ^{27}Al (**a**) and ^{29}Si (**b**) MAS NMR spectra of in-house and as-synthesised mordenite

24 %, compared with 71 % for the isomer products, and thereafter the catalyst was almost deactivated after 240 min on stream. On the other hand, greater TOS stability was shown by the 1 wt% Pt/690HOA and steamed mordenite catalysts. However, a shorter coking rate was observed for the steamed mordenite, so it preserved its initial activity for almost 24 h, after which it deactivated at the rate of 8–10 wt% every day before achieving a pseudo-stable state at the end of the reaction. In contrast, the 1 wt% Pt/690HOA catalyst deactivated continuously from the point when the feed was introduced to the reactor at the slower rate of 3–5 wt% every day, before achieving a pseudo-stable state at the end of the reaction. In addition, selectivity towards C7 isomers and cyclic products for both catalysts was in the range of 97–98 and 2–3 %, respectively.

Faster deactivation and the mono-dimensional pore system of 1 wt% Pt/CBV21, coupled with a higher density of strong acid sites and as-synthesised zeolite, may have caused the lower activity, which may also be attributable to platinum crystallites blocking the pore openings, as previously reported [35, 53]. There are side pockets in the pore topology of mordenite that match the 12MR and 8MR crossing. The higher number of Brønsted acid sites in the cavities also increases the sensitivity of the 8 MR pores to coking and they can easily fill up and become blocked by carbonaceous deposits [54]. The average lifetime of the carbocations on the surface can be lengthened by strong

Table 12 Acid leaching conditions applied and the main characteristics of samples obtained

Condition	NH_4-MOR (wt)	Acid type	Acid conc. (molar)	Acid, Vol. (ml)	Leaching time (h)	Temp (°C)	XRD crystallinity (%)	NMR Si/Al (mol/mol)	ICP Si/Al (mol/mol)
1	1	HCl	6	50	12	25	71	9.53	–
2	1	HCl	6	50	24	25	73	9.63	–
3	1	HCl	6	100	24	25	74	9.69	–
4	1	HCl	Conc	100	24	120	70	15.32	–
5	1	HNO_3	10	100	16	25	73	9.24	–
6	1	HNO_3	6	50	24	25	70	9.32	–
7	1	HNO_3	Conc	100	24	25	70	9.36	–
8	1	HNO_3	Conc	50	24	25	72	9.39	–
9	1	HNO_3	Conc	100	24	120	78	15.30	–
10	1	HNO_3	6	100	24	120	73	16.09	–
11	1	HNO_3	6	100	48	120	75	16.78	–
12	2	HNO_3	10	100	24	120	70	17.10	–
13	1	HNO_3	10	100	16.5	120	77	17.88	–
14	1	HNO_3	10	100	48	120	74	18.75	–
15	1	HNO_3	10	100	87	120	74	19.13	42.76
16	1	HNO_3	10	100	168	120	76	19.25	–

Table 13 The main characteristics of acid-leached and steamed mordenite samples

Bulk (Si/Al) mol/mol	Framework (Si/Al) (mol/mol)	Crystallinity (%)	Bulk Pt (wt%)	Acidity (mmol g^{-1})	Surface area (m^2 g^{-1})	Pore volume (cm^3 g^{-1})	Pore size (Å)
As-synthesised mordenite							
8.44	9.02	82	–	1.24	406.95	0.17	18.02
Acid-leached mordenite							
42.76	19.13	74	–	0.48	478.85	0.23	26.57
Mordenite steamed at 500 °C							
8.97	20.38	66	–	0.30	419.52	0.21	26.97
Mordenite steamed at 600 °C							
9.06	28.84	64	0.58	0.22	415.00	0.20	26.12
Mordenite steamed at 700 °C							
8.89	∞	67	–	–	404.93	0.20	26.68

acidity and narrow pore diameter, while the diffusion of the branched products can be slowed down. Each of these factors will help to crack the tertiary carbocations that have formed during isomerisation prior to desorption and will assist in the re-adsorption and cracking of the branched paraffins before they leave the pores and enter the gas stream [55].

There are various possible explanations for the slower deactivation of 1 wt% Pt/690HOA and steamed mordenite. First, it may be due to the medium acid strength of the catalysts and their reduced acid site density. Alternatively, it may be due to the balance between acid and metal active sites. It could also be ascribed to the existence of mesopores and to the slight increase in the pore volume, which may be beneficial to the diffusion of bulky moieties. Finally, it may be due to post-synthesised mordenite having smaller crystallites. The last two characteristics can be seen as reducing the resistance of the product molecules to formation and diffusion, resulting in less cracking and deactivation of the catalyst caused either by blockages at the site or by plugging of channels. The method of dealumination applied to the final lattice Si/Al ratio influences catalyst activity. For example, steam dealumination leaves the lattice with aluminium removed as EFAL, whereas samples that are practically free of EFAL can result from acid leaching, so EFAL may have a negative effect by blocking pores and preventing the Pt from being well dispersed during the ion-exchange process. This may explain the deactivation of the 1 wt% Pt/690HOA steamed mordenite catalysts.

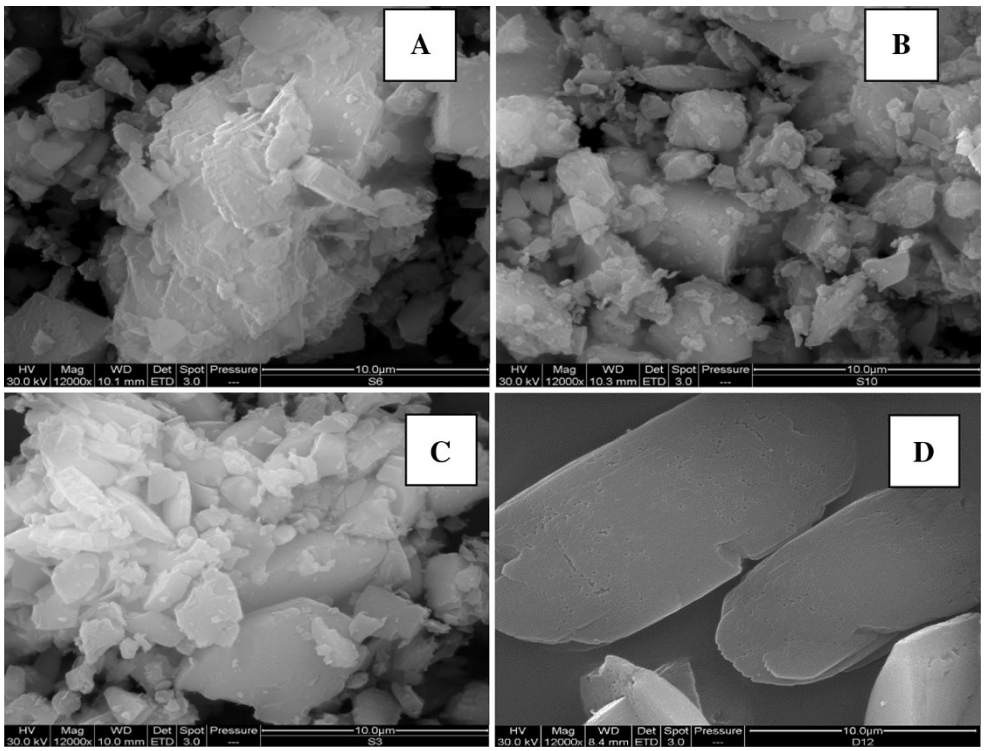

Fig. 25 SEM micrographs of mordenites steamed at 500 °C (**a**), 600 °C (**b**), 700 °C (**c**) and acid leached (**d**)

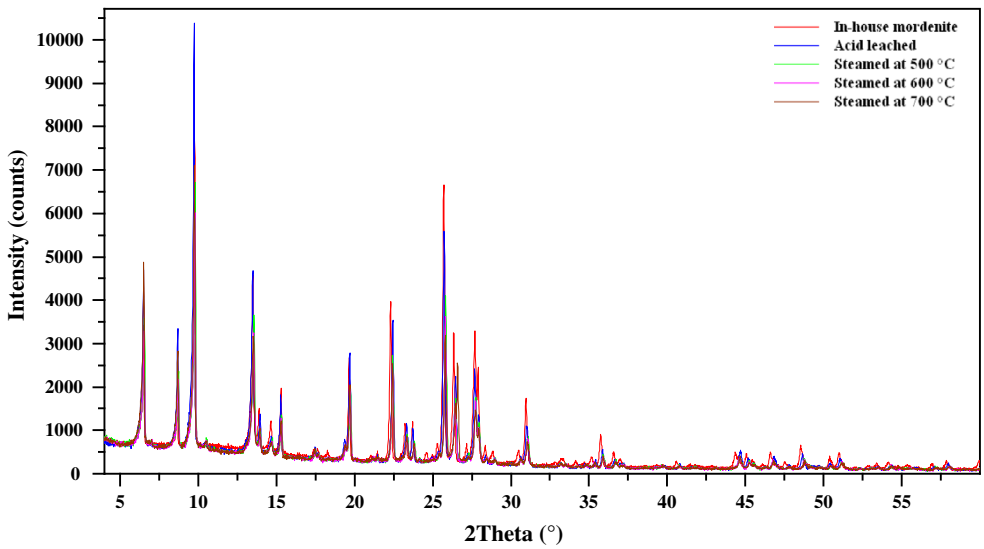

Fig. 26 XRD patterns of acid-leached and steamed mordenites

Deactivation behaviour of two selected commercial mesoporous aluminosilicates and a γ-alumina-based catalyst

TOS stability during the hydroisomerisation of n-C7 under identical reaction conditions was examined using two selected commercial mesoporous aluminosilicates—Al-SBA-15 and Al-MCM-48—and a γ-alumina catalyst, which were loaded with 1 wt% platinum by the ion-exchange technique and tested using the atmospheric pressure glass fixed-bed flow reactor system. The two mesoporous aluminosilicates, Al-SBA-15 and Al-MCM-48, containing 8 and 3 wt% aluminium, respectively, were supplied by Claytec (USA) [20] as white powders in their proton form. Their main surface texture features and the methods by which the alumination and protonation were

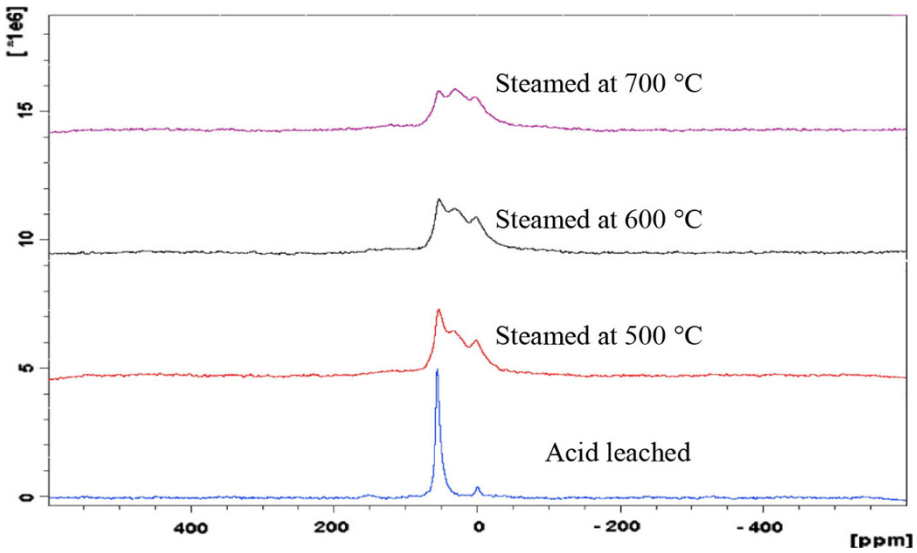

Fig. 27 ^{27}Al NMR of acid-leached and steamed samples

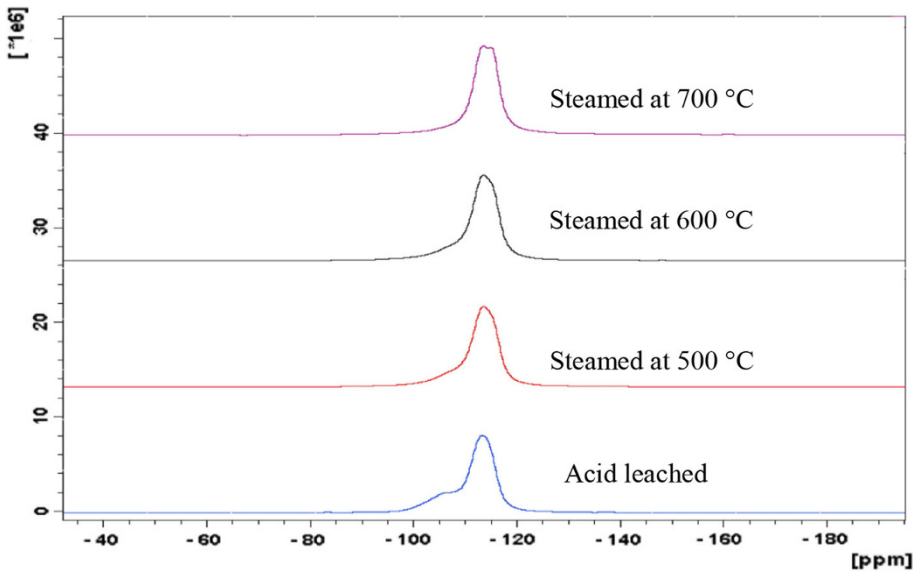

Fig. 28 ^{29}Si NMR of acid-leached and steamed samples

preformed, as specified by the supplier, are shown in Table 14.

Figure 31 shows the SEM image of Al-SBA-15 and Al-MCM-48 catalysts. It can be observed that both samples consist of non-uniform and irregular-shaped particles varying in size from 0.5 to 2 μm. XRD patterns of the Al-SBA-15 and Al-MCM-48 catalysts are shown in Fig. 32. The Al-SBA-15 sample shows well-resolved patterns with a prominent diffraction peak (100) and two additional diffraction peaks indexed to (110) and (200) reflections, which match well with the pattern reported for SBA-15 [56], indicating that the Al-SBA-15 product prepared by post-alumination had a well-ordered hexagonal mesostructure, whereas the XRD pattern of the Al-MCM-48 sample was identical to the one reported by Beck et al. [57]. Four diffraction peaks were also clearly observed and indexed to (211), (220), (420) and (332), indicating that the Al-MCM-48 product prepared by post-alumination had a well-ordered cubic mesostructure. Table 15 shows some in-house characterisations of the Al-SBA-15, Al-MCM-48 and γ-alumina catalysts using various different techniques.

Solid-state MAS NMR spectroscopy of ^{27}Al indicated the presence of tetrahedrally coordinated aluminium atoms in the Al-SBA-15 (A) and Al-MCM-48 lattices. It also revealed extra-framework octahedral and pentahedral Al in the pores of both molecular sieves, which may have been formed during hydrothermal crystallisation and/or by dealumination during calcination [58], as shown in Fig. 33. Therefore, it can be confirmed that not all Al atoms were inserted in the frameworks of SBA-15 and MCM-48.

In the ^{29}Si MAS NMR spectra, two peaks at 110 and 102 ppm were assigned to Si(0Al) and Si(1Al)

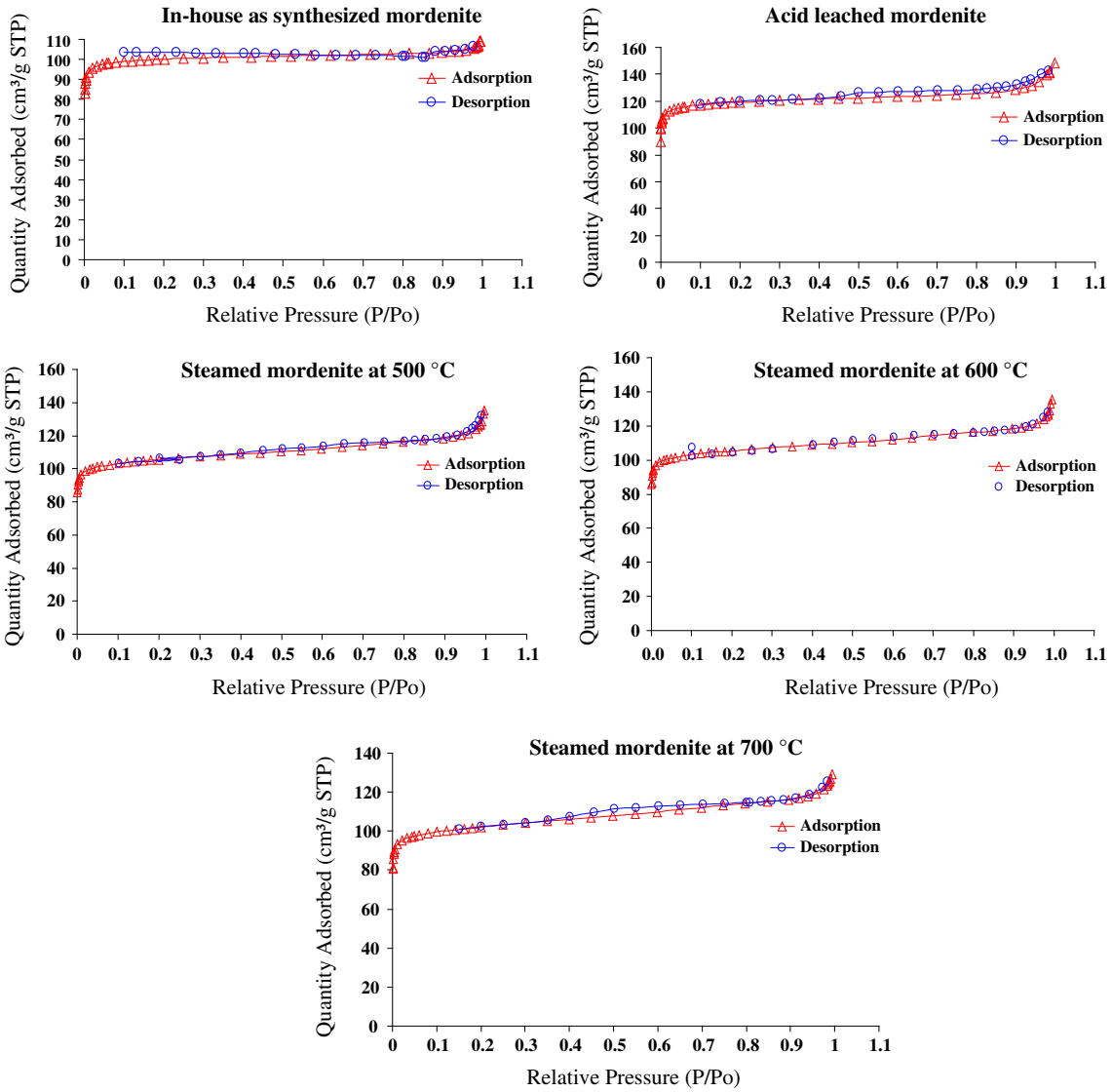

Fig. 29 N_2 adsorption and desorption isotherms of acid-leached and steamed samples

configurations respectively for Al-SBA-15, and three peaks at 110, 101, and 92 ppm were assigned to Si(0Al), Si(1Al) and Si(2Al) configurations respectively for Al-MCM-48, as shown in Fig. 34. This confirmed that some Si atoms were substituted by Al atoms to generate the mesoporous aluminosilicate structure for both catalysts.

The Al-SBA-15 and Al-MCM-48 catalysts were also characterised using nitrogen adsorption at −196 °C, as shown in Fig. 35, to confirm that these materials had retained their mesostructures after the post-alumination process to substitute the silicon with aluminium. Figure 35 shows the nitrogen adsorption isotherms for both catalysts, which are type IV according to the IUPAC classification [59]. The isotherm of the mesoporous molecular sieve exhibits a sharp inflection characteristic of capillary condensation within uniform pores, where the P/P_0 position of the inflection point is related to the diameter of the pore. The sharp rise near 0.4 P/P_0 corresponds to condensation in the primary mesopores. As the size of the primary mesopores increases, the capillary condensation step shifts to higher relative pressures and hysteresis becomes more pronounced. The existence of a hysteresis loop in the isotherms indicates the presence of mesopores and its shape is related to their shape: roughly, a vertical loop indicates cylindrical mesopores, whereas a horizontal one indicates inkbottle-shaped mesopores [51].

As shown in Tables 14 and 15 alongside Fig. 35, the two commercial catalysts exhibited high pore size and pore volume and retained their mesostructures, even after the post-alumination process. Table 14 shows that Al-SBA-15 had a much lower surface area than expected for mesoporous materials (>1,000 $m^2\ g^{-1}$), which can be explained

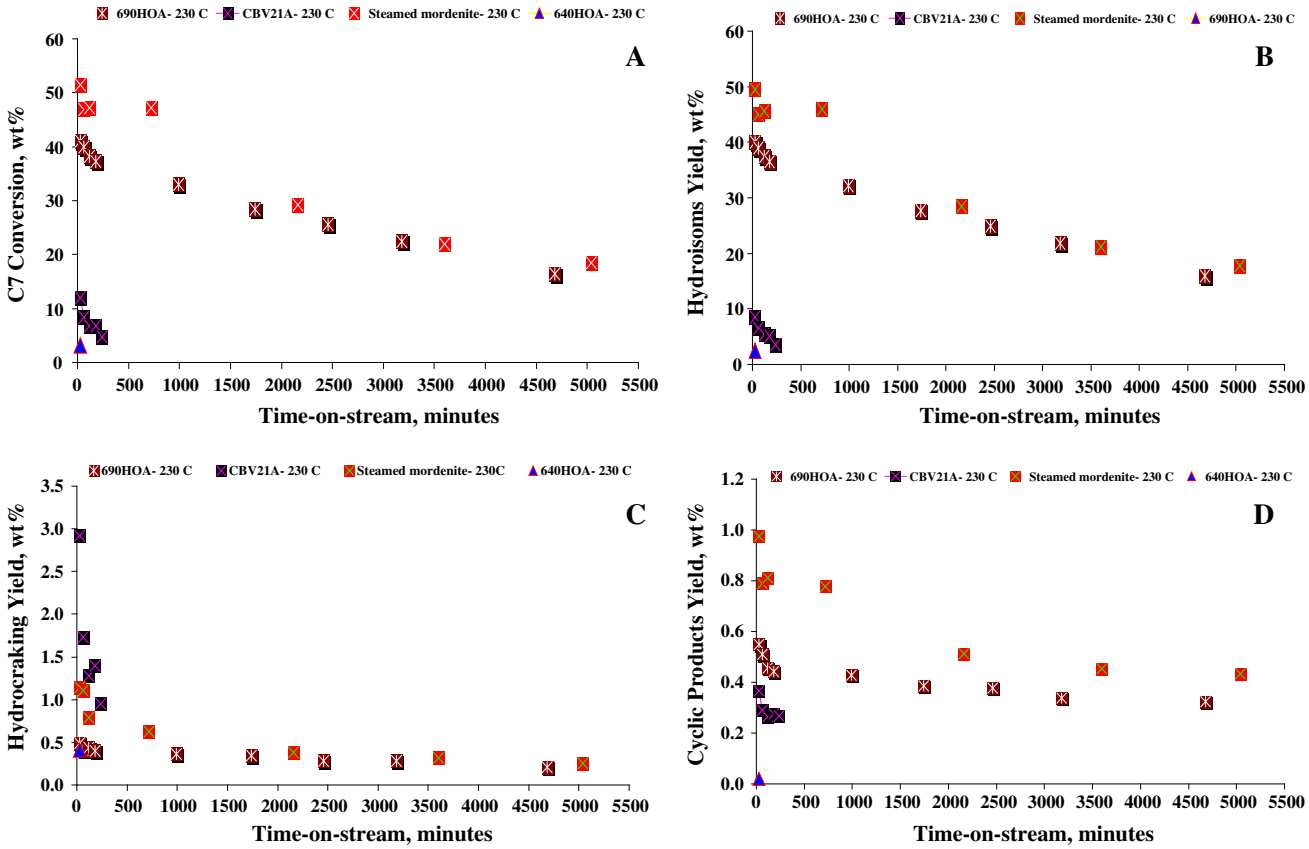

Fig. 30 Overall conversion (**a**), total yield of C7 isomers (mono + di + tribranched isomers) (**b**), total hydrocracking yield (**c**) and total yield of cyclic products (**d**) as a function of TOS for commercial and in-house steamed mordenite catalysts. WHSV = 5.13 h^{-1}; H_2/C7 (mol/mol) = 9; total pressure = 1 atm; temperature = 230 °C; 1 wt% Pt loading

in two ways. First, the presence of EFAL on the mesostructure may partially block the mesopores and subsequently hinder nitrogen adsorption. The existence of EFAL was revealed by NMR, as shown in Fig. 33a. Alternatively, the Al-SBA-15 mesostructure may have partially collapsed, so some residual amorphous material was generated after the post-alumination process. Despite the appearance of the lower surface area, the Al-SBA-15 catalyst retained its general mesostructure, as revealed by the XRD and nitrogen adsorption isotherms shown in Figs. 32 and 35 respectively, while its large pore size and pore volume were comparable with those of Al-MCM-48.

The deactivation behaviour of the 1 wt% Pt/Al-SBA-15 and 1 wt% Pt/Al-MCM-48 catalysts was investigated during the catalytic conversion of n-C7 at reaction temperatures of 210, 230, 250 and 270 °C and at atmospheric pressure, using the glass fixed-bed flow reactor system loaded with 1 g of each catalyst, as described in "Results and discussion" section. The constant mole ratio of hydrogen to n-C7 was 9 and WHSV was 5.13 h^{-1}. At temperatures below 300 °C, very low n-C7 conversion was found, and so 370 °C was chosen as the optimum temperature for studying the activity decay of these catalysts. Figure 36a–d illustrates the effects of TOS on the C7 conversion, hydroisomerisation, hydrocracking and cyclic product yields at reaction temperature of 370 °C for the two catalysts loaded with 1 wt% Pt by the ion-exchange method. The γ-alumina support supplied by Alfa-Aesar (Johnson–Matthey) was also loaded with 1 wt% Pt using the wet impregnation method and tested under the same reaction conditions.

Initially, the respective overall conversions for 1 wt% Pt/Al-SBA-15, 1 wt% Pt/Al-MCM-48 and 1 wt% Pt/γ-Al_2O_3 were 51, 39 and 24 wt%, 30 min after the introduction of feed to the reactor at 370 °C. The 1 wt% Pt/Al-SBA-15 catalyst deactivated slightly with TOS, reaching a conversion of 25 wt% (<26 wt% of the initial catalytic activity) after about 2 days, then remained in a pseudo-stable state until the reaction terminated after 4 days. The 1 wt% Pt/Al-MCM-48 started with less activity than the 1 wt% Pt/Al-SBA-15, but with greater TOS stability, deactivating slightly to reach a conversion of 30 wt% (<9 wt% of the initial catalytic activity) after 2 days, then maintained a pseudo-stable state until the reaction terminated after 3 days. Deactivation was rapid for the 1 wt% Pt/γ-Al_2O_3 catalyst, with high cyclisation activity under the

conditions of the investigation, resulting in selectivity towards the cyclic products at 55 %, compared with 40 % for the isomer products; thereafter, the catalyst was almost deactivated after 180 min on stream. The 1 wt% Pt/Al-SBA-15 and 1 wt% Pt/Al-MCM-48 catalysts also exhibited fairly high cyclisation selectivity, of 20 and 27 wt%, respectively, decreasing with TOS to 7 and 9 wt%, respectively, by the end of the reactions. The cracking selectivity of the 1 wt% Pt/Al-SBA-15, 1 wt% Pt/Al-MCM-48 and 1 wt% Pt/γ-Al_2O_3 catalysts was 1, 3 and 10 wt%, respectively. The maximum isomer yields for 1 wt% Pt/Al-SBA-15, 1 wt% Pt/Al-MCM-48 and 1 wt% Pt/γ-Al_2O_3 were found to be 40, 27 and 10 wt%, respectively, decreasing with TOS in the same way as conversion.

As the major reactions were hydroisomerisation and cyclisation, negligible cracking was observed for the

Table 14 Main surface texture features and the alumination and protonation methods of Al-SBA-15 and Al-MCM-48 as supplied by Claytec (USA) [20]

Sample	BET surface area ($m^2\ g^{-1}$)	Total pore volume @ $P/P_0 = 0.98$ ($cm^3\ g^{-1}$)	BJH pore size (nm)	Alumination and protonation methods
8 wt% Al-SBA-15	408	0.75	8.6	Calcination of the as-made pure silica mesophase at 600 °C to remove surfactant, followed by grafting reaction of the pure silica mesophase with aluminium i-propoxide to achieve alumination, followed by another calcination at 550 °C to form the protonated derivative
3 wt% Al-MCM-48	1,217	1.4	2.4	Sodium aluminate was used for Al incorporation during framework assembly, followed by ammonium ion exchange in the presence of surfactant, then calcination at 600 °C to form the protonated derivative

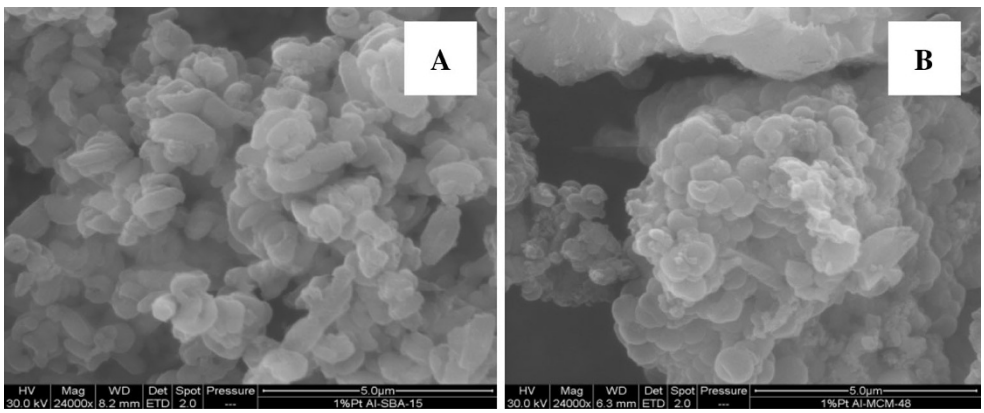

Fig. 31 SEM micrographs of Al-SBA-15 (**a**) and Al-MCM-48 (**b**)

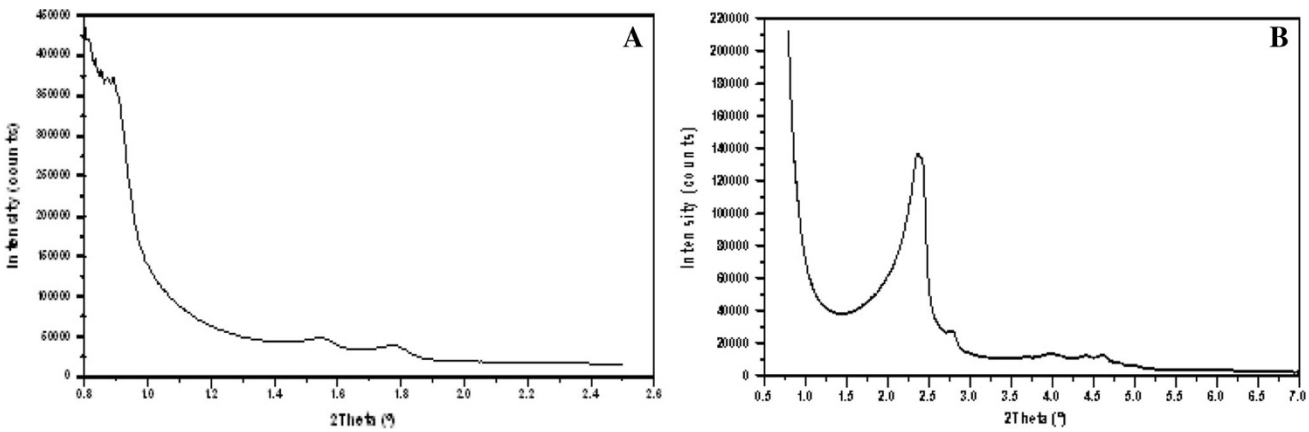

Fig. 32 XRD patterns of Al-SBA-15 (**a**) and Al-MCM-48 (**b**)

Table 15 Some characterisations of Al-SBA-15 and Al-MCM-48 catalysts

Bulk (Si/Al) (mol/mol)	Framework (Si/Al) (mol/mol)	Bulk Pt (wt%)	Si/Al atomic conc % (XPS)	Pt atomic conc % (XPS)	Acidity (mmol g^{-1})	Surface area (m^2 g^{-1})	Pore volume (cm^3 g^{-1})	Pore size (Å)
Al-SBA-15								
11.05	6.39	0.95	10.62	0.04	0.29	–	–	–
Al-MCM-48								
32.65	9.33	0.95	–	–	–	1,035	1.33	34.36
γ-alumina								
–	–	–	–	–	0.19	211	0.59	90.49

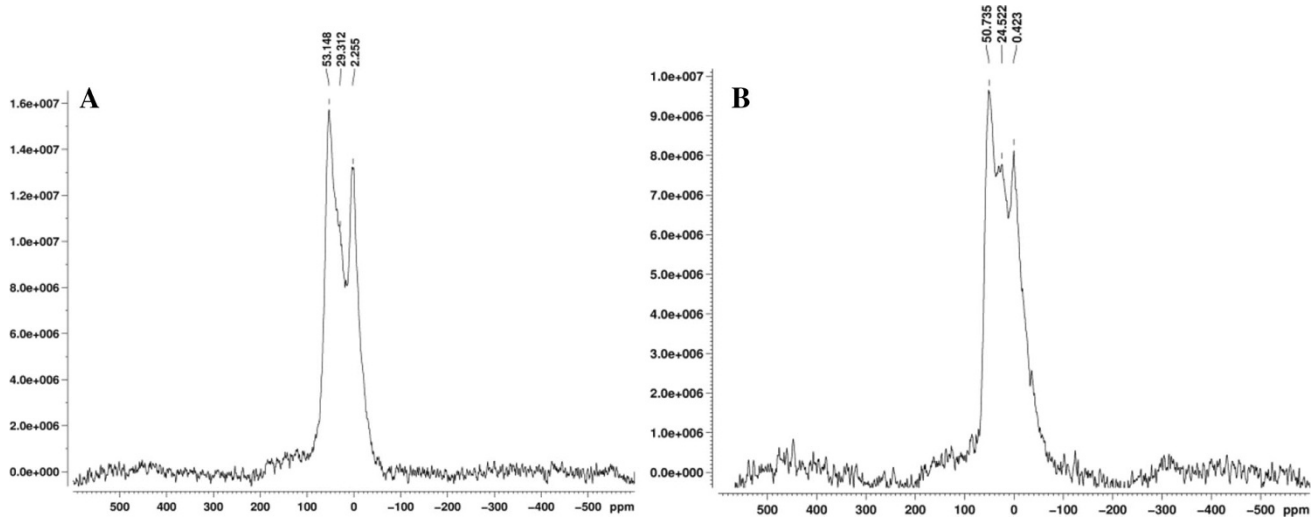

Fig. 33 ^{27}Al MAS NMR spectra of Al-SBA-15 (**a**) and Al-MCM-48 (**b**)

1 wt% Pt/Al-SBA-15 and 1 wt% Pt/Al-MCM-48. Small amounts of alkenes were also detected in the products. Although the deactivation rate was significant during the first few minutes, the activity of the catalyst became reasonably stable after about 2 days. A certain amount of initial deactivation has been reported by other workers during the isomerisation of *n*-alkanes over Pt catalysts, which is expected under atmospheric pressure conditions [60]. However, it was shown that a great quantity of oligomers (cyclic products) is produced from propene at low temperatures on MCM-41-type catalysts and that the pore size of the mesoporous material can make a difference when the aim is to oligomerise larger olefins or to produce large lubricant molecules in general [12].

It is reported that the very high surface area of ordered mesoporous materials makes it easier to obtain highly dispersed noble metal catalysts [12, 61]. However, because these catalysts have fewer acid sites, as shown in Table 15, the turnover frequency (TOF) of n-C7 hydroisomerisation at 370 °C over these sites would be expected to be low, which means in turn that there would be a relatively low level of interaction between the low acid sites in the large pore walls of these catalyst and the iso-heptane molecules generated by dehydrogenation on the platinum sites. Thus, these alkenes will be oligomerated to produce the cyclic products. It can be concluded that the acid and metal sites are not sufficiently well balanced to produce ideal bifunctional catalysts for n-C7 conversion. The oligomers formed may be attributed to the formation of carbonaceous species on the catalyst surface, which contribute to the poisoning and/or blocking of the active centres. Thus, it is clear that good isomerisation activity is obtained when the hydrogenation activity of the metal (Pt) and the Brønsted acid activity of the bifunctional catalyst are in balance. In comparison to the 1 wt% Pt/γ-Al_2O_3 catalyst, the 1 wt% Pt/Al-SBA-15 and 1 wt% Pt/Al-MCM-48 produced smaller quantities of cracked products, probably due to their effectively greater Pt dispersion.

The maximum coke content for the 1 wt% Pt/Al-SBA-15 catalyst was found to be 0.49, 0.72, and 0.70 wt% in the top, middle and bottom reactor zones, respectively, while the minimum coke content for the 1 wt% Pt/γ-Al_2O_3 catalyst was found to be 0.36 wt%, as revealed by TGA analysis. It can be clearly seen that the middle and bottom

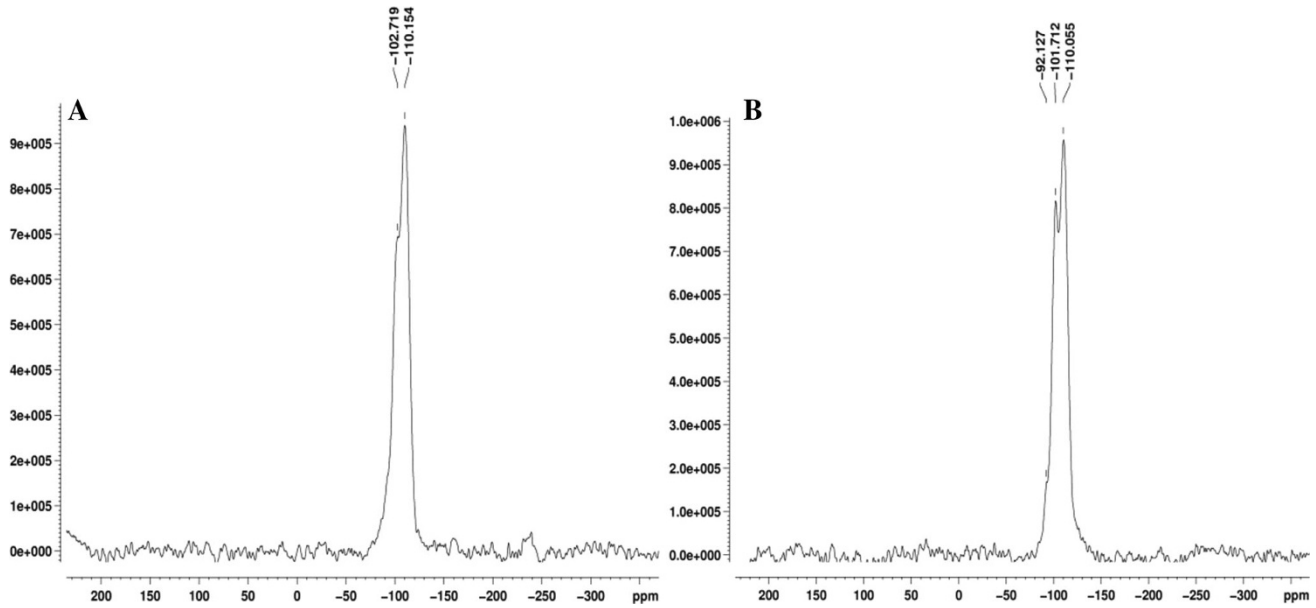

Fig. 34 ^{29}Si MAS NMR spectra of Al-SBA-15 (**a**) and Al-MCM-48 (**b**)

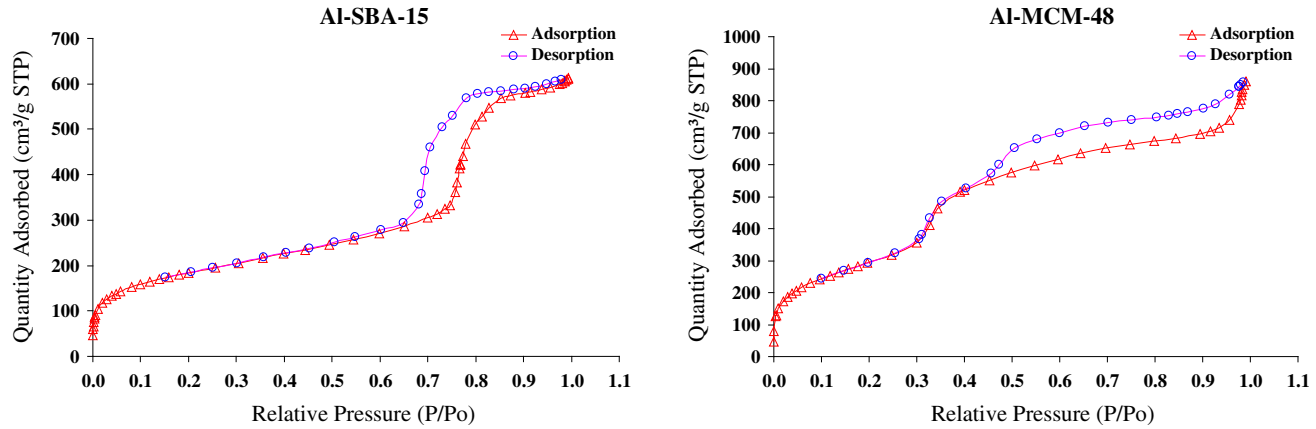

Fig. 35 N_2 adsorption and desorption isotherms of Al-SBA-15 and Al-MCM-48

zones of 1 wt% Pt/Al-SBA-15 had the highest hard coke content in the catalyst bed, whereas there was slightly less coke in the top zone. This suggests that the middle and bottom zones of the catalyst bed contributed the most activity, where the reaction took place. In addition, the lower coke content in the top zone is to some extent indicative of the low acidity of this catalyst and the fact that no diffusion limitations were encountered with it, since such limitations would result in coking and would cause the top section of the bed to be coke rich.

Conclusions

There are many conclusions which can be drawn from this investigation of the deactivation of a range of commercial bifunctional nanoporous-based catalysts during the hydroisomerisation of normal heptane (n-C7) under identical reaction conditions. The main cause of deactivation of acid zeolite catalysts is generally coking, as coke compounds become trapped in the zeolite pores and can poison the acid sites or block their access:

- It has been shown that many different parameters control the stability of USY zeolites in the hydroisomerisation of n-C7. Not only reaction conditions but also catalyst characteristics play the crucial roles.
- For most of the catalysts studied, total conversion increased dramatically as reaction temperature increased in the range of 210–270 °C. However, the total selectivity of C7 isomers at lower temperatures was very high throughout the deactivation reaction at

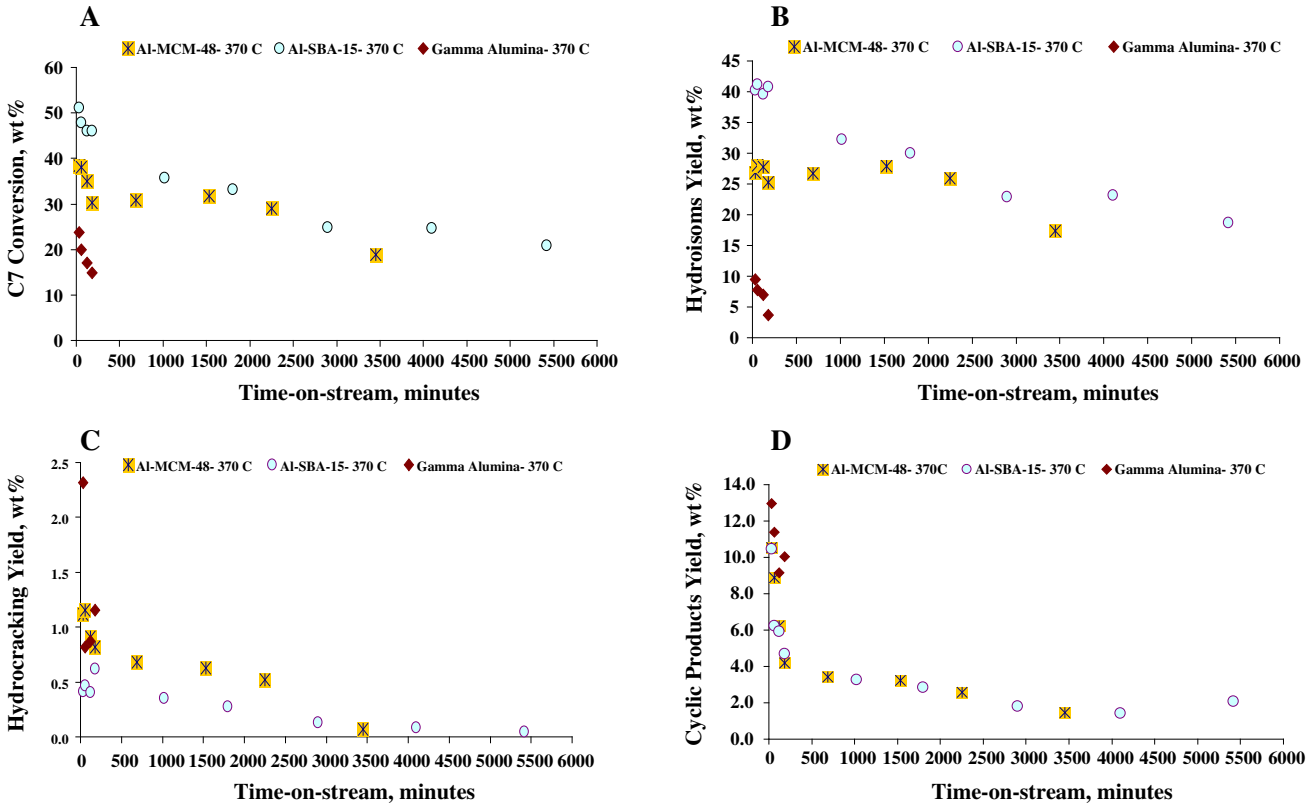

Fig. 36 Overall conversion (**a**), total yield of C7 isomers (mono + di + tribranched isomers) (**b**), total hydrocracking yield (**c**) and total yield of the cyclic products (**d**) as a function of TOS for the Al-SBA-15, Al-MCM-48 and γ-alumina catalysts. WHSV = 5.13 h^{-1}; H_2/C7 (mol/mol) = 9; total pressure = 1 atm; temperature = 370 °C; 1 wt% Pt loading

210 and 230 °C, taking advantage of the thermodynamic equilibrium.

- The selectivity of cracked products increased at the higher temperatures of 250 and 270 °C during the first few hours of the deactivation reaction and then decreased rapidly throughout the TOS. The selectivity of cyclic products was slightly higher at the lower temperatures of 210 and 230 °C.
- Increasing pressure resulted in decreased overall conversion and slightly decreased selectivity to isomers with noticeable increased selectivity to the cyclic products, particularly at the lower temperatures of 210 and 230 °C.
- There was no obvious cracking activity at the lower temperatures of 210 and 230 °C, and constant WHSV as the reaction pressure changed, and in contrast there was increased selectivity towards the cracked product as the reaction pressure increased at the highest temperature of 270 °C.
- The total conversion increased as the contact time increased at constant temperature and pressure. However, increasing the contact time between the n-C7 feed and the catalyst seems to cause an increase in cracking selectivity.
- Zeolite Y commercial catalysts that were generated by steaming at different levels of severity behaved very differently to each other and to acid-leached commercial catalysts.
- USY zeolite pore structures which can inhibit coke formation in conjunction with careful dealumination to decrease the number of acid sites are necessary for the development of time-stable reforming zeolite-based catalysts.
- There is a clear correlation between the obtained yield of the cracked products, which relates to the existence of the stronger acid sites and to the hard coke. Maximum hard coke values were found at 270 °C.
- The balance between the number of Pt atoms and the number of acid sites plays an important role in determining the activity, selectivity and stability of the bifunctional catalyst. The greater the value of n_{Pt}/n_A, the slower the coke formation and the higher the catalyst stability.
- Lower platinum dispersion may have resulted in the formation of a considerably greater quantity of coke.
- Lower acidity, hence less cracking activity, resulted in the catalyst being more stable against deactivation by coking, which is the case for zeolites with high Si/Al ratios.

- High surface area and larger pore volume, due to the more severe dealumination process and acid leaching, reduced the hard coke content, thus slowing the deactivation rate.
- The AHFS acid-leached zeolite had a larger pore volume (smaller pore size and larger surface area), due to the alleviation of the obstruction by EFAL of the mesopore system, thus slowing the formation of coke and providing good catalytic stability.
- The higher Pt loading, up to 2 wt%, improved catalytic stability, due to a better balance and closeness of the catalytic functions.
- Pt–Ni bimetallic catalysts were better than monometallic catalysts containing only Ni because they had higher activity, better selectivity for C7 isomers and more stability. The presence of platinum in the bimetallic catalysts improved the formation of metal particles to a great extent and reduced their sizes, while enhancing the reduction of nickel.
- The best method to introduce the platinum into the beta zeolite pores was found to be the ion-exchange method at pH > 9 which achieved a better metal/acid balance, lower cracking activity, and relatively good metal dispersion.
- The metal functions deactivated faster than the acid functions for all the catalysts loaded with platinum, irrespective of the method used. However, this was not sufficiently severe to cause a drop in n-C7 conversion due to the unique channel system and pore structure of beta zeolite.
- The TOS behaviour of USY zeolites can be enhanced by forming composite catalysts of USY and beta zeolite, providing a unique pore structure and acidity to improve their TOS stability.
- The metal function deactivated faster than the acid function in all the composite catalysts but did not cause a severe drop in n-C7 conversion, indicating that the composite zeolite pore structure plays a very important role in the conversion, and an appropriate combination of the pore structure and acidity showed superior TOS behaviour.
- Although the composite catalyst offers a highest acidity compared to the corresponding individual catalysts; coking is moderate and as such the TOS stability is reasonable.
- Synthesis parameters greatly affect mordenite morphology in terms of the size and aspect ratio of the mordenite crystals, so a range of mordenite morphologies were obtained for a variety of catalysts, both in-house and commercial. Each catalyst had different diffusion and porosity properties; therefore, performance differed among them.
- The framework aluminium was removed to extra-framework positions as a result of steam dealumination as well as giving the final in-framework Si/Al ratio. On the other hand, acid leaching resulted in samples that were practically free of EFAL, which in turn led to the formation of aluminium gradients along the zeolite crystallites. A more uniform aluminium distribution was achieved by steam treatment.
- The main factors controlling catalyst stability and selectivity were pore topology, acid strength, acid site density and location of the acid sites. The crucial feature for coke formation was the pore topology of the catalyst.
- The synthesis method of mesoporous materials and the post-alumination process applied significantly affect the number and strength of acid sites and thereby their catalytic activity, selectivity and stability.
- As the mesoporous molecular sieves present very high total surface area and large pore size, this may depress the TOF, causing the olefins (alkenes) produced during the dehydrogenation of alkanes on the metal sites to have less interaction with the acid sites on which they can be hydrogenated to give their relevant isomers. Thus, the alkenes will be oligomerated to produce the cyclic products, which may be attributed to the formation of carbonaceous species on the catalyst surface, contributing to the poisoning and/or blocking of the active centres.

Acknowledgments I would like to thank Dr. Patrick Hill (Manchester University) for his help in carrying out the SEM analysis, Dr. Vladimir Zholobenk (Keele University) who kindly provided the FTIR technique, Dr. Christopher Muryn (Manchester University) for his help in performing the XRD analyses, Professor Michael Anderson and Dr. Barbara Gore (Manchester University), who kindly provided the NMR technique, Mr. Martin Jennings (Manchester University) for his help with the elemental analysis and Mr. David Gordon (Manchester University) for his cooperation in making the glass reactor.

References

1. Guisnet M, Ribeiro FR (2011) Deactivation and regeneration of zeolite catalysts. Imperial College Press, London
2. Bartholomew CH (2003) Catalyst deactivation and regeneration. In: Kirk-Othmer encyclopedia of chemical technology. Wiley, London
3. Zhang W, Smirniotis PG (1999) On the exceptional time-on-stream stability of HZSM-12 zeolite: relation between zeolite pore structure and activity. Catal Lett 60:223–228

4. Stöcker M (2005) Gas phase catalysis by zeolites. Microporous Mesoporous Mater 82:257–292
5. Gopal S, Smirniotis PG (2004) Factors affecting isomer yield for *n*-heptane hydroisomerization over as-synthesized and dealuminated zeolite catalysts loaded with platinum. J Catal 225:278–287
6. Kuznetsov PN (2003) Study of *n*-octane hydrocracking and hydroisomerization over Pt/HY zeolites using the reactors of different configurations. J Catal 218:12–23
7. Villegas JI, Kumar N, Heikkila T, Smieskova A, Hudec P, Salmi T, Murzin DY (2005) A highly stable and selective Pt-modified mordenite catalyst for the skeletal isomerization of n butane. Appl Catal 284:223–230
8. McDaniel CW, Maher PK (1968) New ultrastable form of faujasite. In: Molecular sieves. London: Soc Chem Ind, pp 86–194
9. Van Laak ANC, Sagala SL, Zečević J, Friedrich H, de Jongh PE, de Jong KP (2010) Mesoporous mordenites obtained by sequential acid and alkaline treatments—catalysts for cumene production with enhanced accessibility. J Catal 276:170–180
10. Moushey DL (2006) Formation of mesoporosity in zeolite and mesoporous molecular sieve structures through use of carbon as a secondary templating agent. Dissertation, University of Cincinnati, USA
11. Logar NZ, Kaucic V (2006) Nanoporous materials: from catalysis and hydrogen storage to wastewater treatment. Acta Chim Slov 53:117–135
12. Corma A (1997) From microporous to mesoporous molecular sieve materials and their use in catalysis. Chem Rev 97:2373–2419
13. Pinnavaia TJ, Liu Y (2002) Aluminosilicate mesostructures with improved acidity and hydrothermal stability. J Mater Chem 12:3179–3190
14. Zeolyst International, http://www.zeolyst.com/our-products/standard-zeolite-powders/zeolite-y.aspx. Accessed 29 May 2011
15. Tosoh Corporation, http://www.tosoh.com/Products/tcdzeo.htm#hzc. Accessed 26 June 2011
16. Rawlence DJ, Earl, GJ (1993) Materials having novel structure factors for catalysis of hydrocarbon transformation and development of selective processes. BRITE-EURAM 4633, 5th Meeting Report, Elf Solaize
17. Abudawood R, Alotaibi F, Garforth A (2011) Hydroisomerization of *n*-heptane over Pt-loaded USY zeolites. Effect of steaming, dealumination and the resulting structure on catalytic properties. Ind Eng Chem Res 50:9918–9924
18. Abudawood R (2010) Hydroisomerization of alkanes over metal-loaded zeolite catalysts. Dissertation, University of Manchester
19. Alotaibi F (2011) Comparative study of the time-on-stream stability of bifunctional nanoporous-based catalysts in *n*-heptane hydroisomerisation. Dissertation, University of Manchester
20. Claytec, Inc., http://claytecinc.com/products. Accessed 29 May 2011
21. Robson H, Lillerud KP (2001) Verified Syntheses of zeolitic materials, 2nd edn. Elsevier, Amsterdam
22. Weitkamp J, Puppe L (1999) Catalysis and zeolites. Springer, Berlin
23. Wang QL, Torrealba M, Giannetto G, Guisnet M, Perot G, Cahoreau M, Caisso J (1990) Dealumination of Y zeolite with ammonium hexafluorosilicate: a SIM-XPS study of the aluminium distribution. Zeolites 10:703–706
24. Wang QL, Giannetto G, Torreaaba M, Perot G, Kappenstein C, Guisnet M (1991) Dealumination of zeolites: II. Kinetic study of the dealumination by hydrothermal treatment of a NH4NaY zeolite. J Catal 130:459–470
25. Wang QL, Giannetto G, Guisnet M (1991) Dealumination of zeolites: III. Effect of extra-framework aluminum species on the activity, selectivity, and stability of Y zeolites in *n*-heptane cracking. J Catal 130:471–482
26. Remy MJ, Stanica D, Poncelet G, Feijen EJP, Grobet PJ, Martens JA, Jacobs PA (1996) Dealuminated H–Y zeolites: relation between physicochemical properties and catalytic activity in heptane and decane isomerization. J Phys Chem 100:12440–12447
27. Van Bekkum H, Flanigen EM, Jacobs PA, Jansen JC (2001) Introduction to zeolite science and practice, 2nd edn. Elsevier, Amsterdam, pp 261–288
28. Roussel ML, emberton J, Guisnet M, Cseri T, Benazzi E (2003) Mechanisms of *n*-decane hydrocracking on a sulfided NiW on silica–alumina catalyst. J Catal 218: 427–437
29. Guerin M, Kappenstein C, Alvarez F, Giannetto G, Guisnet M (1988) Preparation of PtHY catalysts: influence on the catalytic properties of the complexes used as platinum precursors. Appl Catal 45:325–333
30. Martins A, Silva JM, Ribeiro FR, Ribeiro MF (2006) Hydroisomerization of *n*-hexane over Pt–Ni/HBEA using catalysts prepared by different methods. Catal Lett 109(1–2):83–87
31. Alotaibi F, Abudawood R, Al-Megren H, Al-Kinany H, Garforth A (2013) The time-on-stream stability of some selected bifunctional nanoporous-based catalysts in *n*-heptane hydroisomerisation. J Appl Petrochem Res (submitted)
32. Chao K, Lin C, Lin C, Wu H, Tseng C, Chen S (2000) *n*-Heptane hydroconversion on platinum-loaded mordenite and beta zeolites: the effect of reaction pressure. Appl Catal A 203:211–220
33. Tran MT, Gnep NS, Szabo G, Guisnet M (1998) Isomerization of *n*-butane over H-mordenites under nitrogen and hydrogen: influence of the acid site density. J Catal 174:185–190
34. Guisnet M, Fouche V (1991) Isomerization of *n*-hexane on platinum dealuminated mordenite catalysts: I. Influence of the silicon-to-aluminium ratio of the zeolite. Appl Catal 71:283–293
35. Wang ZB, Kamo A, Yoneda T, Komatsu T, Yashima T (1997) Isomerization of *n*-heptane over Pt-loaded zeolite β catalysts. Appl Catal 159:119–132
36. Chica A, Corma A (1999) Hydroisomerization of pentane, hexane, and heptane for improving the octane number of gasoline. J Catal 187:167–176
37. Lónyi F, Lunsford JH (1992) The development of strong acidity in hexafluorosilicate-modified Y-type zeolites. J Catal 136:566–577
38. Cruz JM, Corma A, Fornes V (1989) Framework and extra-framework aluminum distribution in $(NH_4)_2F_6Si$-dealuminated Y-zeolites—relevance to cracking catalysts. Appl Catal 50:287–293
39. Gola A, Rebours B, Milazzo E, Lynch J, Benazzi E, Lacombe S, Delevoye L, Fernandez C (2000) Effect of leaching agent in the dealumination of stabilized Y zeolites. Microporous Mesoporous Mater 40:73–83
40. Jordao MH, Valencia E, Vicemario S, Dilson C (1999) Characterization of Pt/HUSY and Pt-Ni/HUSY catalysts by transmission electron microscopy. Mate Res 2:219–223
41. Karthikeyan D, Lingappan N, Sivasankar B (2008) Hydroisomerization of *n*-octane over bifunctional Ni-Pd/HY zeolite catalysts. Ind Eng Chem Res 47:6538–6546
42. Barsi FV, Cardoso D (2009) Bimetallic Pt–Ni catalysts supported on USY zeolite for *n*-hexane isomerization. Braz J Chem Eng 26–2:353–360
43. Roldán R, Beale AM, Sánchez-Sánchez M, Romero-Salguero FJ, Jiménez-Sanchidrián C, Gómez JP, Sankar G (2008) Effect of the impregnation order on the nature of metal particles of bi-functional Pt/Pd-supported zeolite beta materials and on their catalytic activity for the hydroisomerization of alkanes. J Catal 254:12–26
44. Eswaramoorthi I, Lingappan N (2003) Ni–Pt/H–Y zeolite catalysts for hydroisomerization of *n*-hexane and *n*-heptane. Catal Lett 87(3–4):133–142
45. Kampers FWH, Engelen CWR, van Hoof JHC, Konigsberger DC (1990) Influence of preparation method on the metal cluster size

of platinum/ZSM-5 catalysts as studied with EXAFS. J Phys Chem 94(23):8574–8578
46. Changlei J, Bo M, Xiwen Z, Fengxiang L, Zhizhi Z, Bo Q (2008) Catalytic performance of Pt/HY-β in *n*-octane hydroisomerization. Petrol Sci 6:299–305
47. Smirniotis PG, Davydov L, Ruckenstein E (1999) Composite zeolite-based catalysts and sorbents. Catal Rev 41:43–113
48. Hamidi F, Bengueddach A, Di Renzo F, Fajula F (2003) Control of crystal size and morphology of mordenite. Catal Lett 87:149–152
49. Treacy MMJ, Higgins JB (2001) Collection of simulated XRD powder patterns for zeolites. Elsevier, Amsterdam
50. Janssen AH, Koster AJ, de Jong KP (2001) Three-dimensional transmission electron microscopy observations of mesopores in dealuminated zeolite Y. Angew Chem Int Ed 40:1102–1104
51. Van Donk S, Janssen AH, Bitter JH, de Jong KP (2003) Generation, characterization, and impact of mesopores in zeolite catalysts. Catal Rev 45:297–319
52. Janssen AH, Koster AJ, de Jong KP (2002) On the shape of the mesopores in zeolite Y: a three-dimensional transmission electron microscopy study combined with texture analysis. J Phys Chem 106:11905–11909
53. Lee JK, Rhee HK (1997) Characteristics of Pt/H-beta and Pt/H-mordenite catalysts for the isomerization of *n*-hexane. Catal Today 38:235–242
54. Van Donk S (2002) Adsorption, diffusion and reaction studies of hydrocarbons on zeolite catalysts. PhD Dissertation, Utrecht University, Netherlands
55. Chica A, Corma A, Miguel PJ (2001) Isomerization of C5–C7 *n*-alkanes on unidirectional large pore zeolites: activity, selectivity and adsorption features. Catal Today 65:101–110
56. Nie C, Huang L, Zhao D, Li Q (2001) Performance of Pt/Al-SBA-15 catalysts in hydroisomerization of *n*-dodecane. Catal Lett 71:117–125
57. Beck JS, Vartuli JC, Roth WJ, Leonowicz ME, Kresge CT, Schmitt KD, Chu CTW, Olson DH, Sheppard EW (1992) A new family of mesoporous molecular sieves prepared with liquid crystal templates. J Am Chem Soc 114:10834–10843
58. Eimer GA, Pierella LB, Monti GA, Anunziata OA (2002) Synthesis and characterization of Al-MCM-41 and Al-MCM-48 mesoporous materials. Catal Lett 78:65–75
59. Gregg SJ, Sing KSW (1982) Adsorption, surface area and porosity. Academic Press, London
60. Chaudhari K, Das TK, Chandwadkar AJ, Sivasanker S (1999) Mesoporous aluminosilicate of the MCM-41 type: its catalytic activity in *n*-hexane isomerization. J Catal 186:81–90
61. Chaudhari K (2000) Synthesis, characterization and catalytic properties of mesoporous molecular sieves. PhD Thesis, Catalysis Division, National Chemical Laboratory, Pune